

Generalization with data-dependent quantum geometry

Tobias Haug^{1,2,*} and M. S. Kim²

¹Quantum Research Center, Technology Innovation Institute, Abu Dhabi, UAE

²Blackett Laboratory, Imperial College London SW7 2AZ, UK

Generalization is the ability of machine learning models to make accurate predictions on new data by learning from training data. However, understanding generalization of quantum machine learning models has been a major challenge. Here, we introduce the data quantum Fisher information metric (DQFIM). It describes the capacity of variational quantum algorithms depending on variational ansatz, training data and their symmetries. We apply the DQFIM to quantify circuit parameters and training data needed to successfully train and generalize. Using the dynamical Lie algebra, we explain how to generalize using a low number of training states. Counter-intuitively, breaking symmetries of the training data can help to improve generalization. Finally, we find that out-of-distribution generalization, where training and testing data are drawn from different data distributions, can be better than using the same distribution. Our work provides a useful framework to explore the power of quantum machine learning models.

The key challenge in quantum machine learning is to design models that can learn from data and apply their acquired knowledge to perform well on new data [1]. This latter ability is called generalization and has been intensely studied recently [2–19]. Constructing models that generalize well is essential for quantum machine learning tasks such as learning unitaries [20–27], classification [28, 29], compiling [11, 30, 31], generative modeling [32, 33], quantum simulation [10, 34, 35], quantum autoencoders [36, 37] and black-hole recovery protocols [38]. However, the conditions for generalization are not well understood. Recently proposed uniform generalization bounds [7, 39] have been shown to be loose [40], do not account for symmetries and are unable to explain numerical observations of generalization with few training data [10, 39, 40].

Thus, there is an urgent need for a framework to understand the conditions for successful training and generalization [8, 41–51] to potentially gain advantage over classical models [52–55]. In classical machine learning, generalization has been evaluated using the classical Fisher information [4, 5, 56–58]. Recent works proposed the quantum Fisher information metric (QFIM) to characterize capacity and overparameterization of parameterized quantum states [49, 59–61], however a connection with generalization has not been established.

Here, we introduce the data quantum Fisher information metric (DQFIM) to study generalization and overparameterization. In contrast to the QFIM, the DQFIM correctly captures the effect of data and circuit symmetries on the capacity of quantum machine learning models. The rank of the DQFIM quantifies the circuit depth and amount of data needed for generalization and convergence to a global minimum of the cost function. We apply our methods to learning unitaries, quantum control, generative models, finding excited states and classification tasks. Using the connection between DQFIM and dynamical Lie algebra (DLA), we explain why quantum machine learning can generalize with few training data.

While symmetries have been known to benefit quantum machine learning, we surprisingly find that symmetries in data can also hinder generalization. Finally, we show that out-of-distribution generalization, i.e. the training data is drawn from a different distribution than the test data, can exhibit better performance compared to in-distribution generalization. Our methods provide a quantum geometric picture to understand generalization which guides the design of better quantum machine learning models.

Model.— We consider a unitary $U(\boldsymbol{\theta})$ parameterized by M -dimensional parameter vector $\boldsymbol{\theta}$ and training set $S_L = \{|\psi_\ell\rangle, O_\ell\}_{\ell=1}^L$ of size L . S_L consists of input states $|\psi_\ell\rangle$ drawn from a distribution $|\psi_\ell\rangle \in W$, as well as hermitian operator O_ℓ which represents the label [10, 35, 39]. We now learn by minimizing the cost function

$$C_{\text{train}}(\boldsymbol{\theta}, S_L) = 1 - \frac{1}{L} \sum_{\ell=1}^L \langle \psi_\ell | U(\boldsymbol{\theta})^\dagger O_\ell U(\boldsymbol{\theta}) | \psi_\ell \rangle. \quad (1)$$

Here, we assume without losing generality that the eigenvalues of O_ℓ are (tightly) upper bounded by 1 such that $C_{\text{train}} \geq 0$. The trained model generalizes when the test error in respect to unseen test data $|\psi\rangle \in W$ and corresponding label $O_{|\psi\rangle}$ is small

$$C_{\text{test}}(\boldsymbol{\theta}, W) = 1 - \mathbb{E}_{|\psi\rangle \in W} [\langle \psi | U(\boldsymbol{\theta})^\dagger O_{|\psi\rangle} U(\boldsymbol{\theta}) | \psi \rangle]. \quad (2)$$

Let us now give two important examples of our model: First, unitary learning or quantum compiling aims to represent a target unitary V with a parameterized unitary $U(\boldsymbol{\theta})$ such that $V|\psi_\ell\rangle = U(\boldsymbol{\theta})|\psi_\ell\rangle$ [26, 30]. Here, $|\psi_\ell\rangle$ are initial states with corresponding label operator $O_\ell = V|\psi_\ell\rangle\langle\psi_\ell|V^\dagger$ being the target state to be learned. This learning model also describes quantum control problems [62]. Further, unsupervised generative models to learn a probability distribution $p(x)$ can be converted into unitary learning tasks [63] by encoding empirical distribution $q(x)$ into a state $|\Phi\rangle$ with $q(x) \sim |\langle x | \Phi \rangle|^2$, and choosing $O_\ell = |\Phi\rangle\langle\Phi|$.

Another important task is classification [28]: Here, the goal is to identify two classes, e.g. images of cats and dogs. One encodes the feature vector \mathbf{x}_ℓ into $|\psi_\ell(\mathbf{x}_\ell)\rangle$ with corresponding label $y_\ell = \pm 1$ and label operator $O_\ell = y_\ell \sigma^z$, where cats have $y = 1$ and dogs $y = -1$. The trained model infers the class y by measuring $y \sim \langle \psi | U(\boldsymbol{\theta})^\dagger \sigma^z U(\boldsymbol{\theta}) | \psi \rangle$.

The parameterized ansatz unitary $U(\boldsymbol{\theta}) = \prod_{k=1}^G U^{(k)}(\boldsymbol{\theta}_k)$ commonly consists of G repeating layers of unitaries $U^{(k)}(\boldsymbol{\theta}_k) = \prod_{n=1}^K \exp(-i\theta_{kn} H_n)$, where H_n are hermitian operators, $\boldsymbol{\theta}_k$ a K -dimensional vector, and $\boldsymbol{\theta} = \{\boldsymbol{\theta}_1, \dots, \boldsymbol{\theta}_G\}$ the $M = GK$ dimensional parameter vector [22, 62]. The optimization program starts with a randomly chosen $\boldsymbol{\theta}$ and iteratively minimizes Eq. (1) with the gradient $\nabla C_{\text{train}}(\boldsymbol{\theta})$, which can be efficiently estimated by a quantum computer [64]. Gradient descent iteratively updates $\boldsymbol{\theta} \rightarrow \boldsymbol{\theta} - \alpha \nabla C_{\text{train}}$ with some α until reaching a minimum after E training steps, where $\nabla C_{\text{train}}(\boldsymbol{\theta}^*) = 0$ with converged parameter $\boldsymbol{\theta}^*$. We assume that ansatz $U(\boldsymbol{\theta})$ can solve the learning task, i.e. we ensure that there is a parameter $\boldsymbol{\theta}_g$ such that $C_{\text{test}}(\boldsymbol{\theta}_g, W) = C_{\text{train}}(\boldsymbol{\theta}_g, S_L) = 0$.

After training we have three possible outcomes: (i) Become stuck in local minimum $C_{\text{test}} \geq C_{\text{train}} \gg 0$; (ii) Reach global minimum $C_{\text{train}} \approx 0$, however no generalization with $C_{\text{test}} \gg 0$. (iii) Generalization with $C_{\text{train}} \approx C_{\text{test}} \approx 0$. In the following, we show that the DQFIM determines the critical number of circuit parameters $M_c(L)$ for overparameterization as function of L and training states L_c for generalization.

DQFIM.— First, we define what can be learned about ansatz unitary $U(\boldsymbol{\theta})$ via training set S_L :

Definition 1 (Projected unitary). *The data state for training set $S_L = \{|\psi_\ell\rangle, O_\ell\}_{\ell=1}^L$ of L states is given by*

$$\rho_L = \frac{1}{L} \sum_{\ell=1}^L |\psi_\ell\rangle\langle\psi_\ell| \quad (3)$$

Training with cost function Eq. (1) and S_L gives only information on the unitary projected onto the subspace of the training data $U_L(\boldsymbol{\theta}) \sim U(\boldsymbol{\theta})\rho_L$.

To understand Def. 1, consider the d -dimensional unitary $U \equiv U(\mathbf{u}) = \sum_{n,k=1}^d u_{nk} |n\rangle\langle k|$ with complex parameters $\mathbf{u} = \{u_{11}, u_{12}, \dots, u_{dd}\}$ and training data $\{|\ell\rangle\}_{\ell=1}^L$, where $|\ell\rangle \in W$ are computational basis states and our goal is to learn some unitary $V = U(\mathbf{u}^*)$. For $L = 1$, training with Eq. (1) optimizes $U|1\rangle = \sum_{n=1}^d u_{n1} |n\rangle$. Thus, only the column vector $u_1 = (u_{11}, u_{21}, \dots, u_{d1})$ of U can be trained, while $u_{n>1}$ are not learnable. For arbitrary L , applying U on the training states gives us $\{U|\ell\rangle = \sum_{n=1}^d u_{n\ell} |n\rangle\}_{\ell=1}^L$. The learnable parameters of U correspond to the $d \times L$ -dimensional (unnormalized) isometry $U_L = (u_1, \dots, u_L) \equiv U\rho_L$ with (unnormalized) projector $\rho_L = L^{-1} \sum_{\ell=1}^L |\ell\rangle\langle\ell|$ (see Fig. 1a). Even if we

find a global minima with $C_{\text{train}} = 0$, for $L < d$ we gain no information about the column vectors (u_{L+1}, \dots, u_d) . The trained model $U(\mathbf{u}^*)$ randomly guesses these column vectors, resulting in a large generalization error C_{test} . Only for $L = d$, we have a complete training set that can achieve generalization with $C_{\text{test}} = 0$.

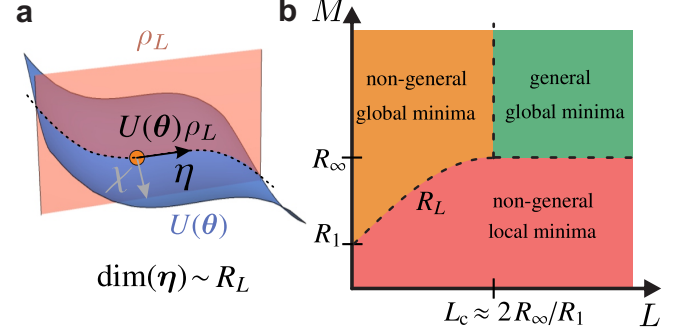


FIG. 1. **a)** Ansatz unitary $U(\boldsymbol{\theta})$ and M -dimensional parameter vector $\boldsymbol{\theta}$ is optimized in respect to cost function Eq. (1) using L training data described by datastate ρ_L (Eq. (3)). Only the subspace of the unitary projected onto the training data $U_L \equiv U(\boldsymbol{\theta})\rho_L$ can be learned. Its learnable degrees of freedom are given by the maximal rank of the data quantum Fisher information metric (DQFIM) R_L . **b)** Phase diagram of generalization with M and L . Convergence to global minimum ($C_{\text{train}} \approx 0$) is likely for overparameterization $M \geq R_L$. Generalization to unseen test data ($C_{\text{test}} \approx 0$) for overcomplete training data when $L \geq L_c \approx 2R_\infty/R_1$ and $M \geq R_\infty$.

To understand generalization, we count the independent parameters of U_L , which we call the effective dimension D_L . For $L = 1$, $U|1\rangle = \sum_{n=1}^d u_{n1} |n\rangle = \sum_{n=1}^d (a_{n1} + ib_{n1}) |n\rangle$ has $2d$ real parameters a_{n1}, b_{n1} . However, due to global phase and norm, there are only $D_1 = 2d - 2$ independent parameters. For $L = d$, parameterizing a complete unitary U requires $D_d = d^2 - 1$ parameters. For example, a single qubit has $D_1 = 2$ (Bloch sphere) and $D_2 = 3$ (arbitrary unitary) free parameters [65], and thus we require $L \geq 2$ states to generalize. However, depending on ansatz and data structure D_L can decrease. Let us consider $U(\boldsymbol{\theta}) = e^{-i\sigma_z \theta_k} \dots e^{-i\sigma_z \theta_M}$ and distribution $W = \{|+\rangle, |-\rangle\}$ with $|\pm\rangle \sim |0\rangle \pm |1\rangle$ and z -Pauli σ_z . While we have M parameters, the generators commute and $L = 1$ is sufficient to generalize as $D_1 = D_d = 1$. In contrast, for $W = \{|0\rangle, |1\rangle\}$ we have $D_L = 0$ as only the trivial global phase is rotated.

We now propose the DQFIM to quantify the effective dimension (see Supplemental materials (SM) A):

Definition 2 (DQFIM). *For unitary $U(\boldsymbol{\theta}) \equiv U$ and training set S_L , the DQFIM is defined as*

$$\mathcal{Q}_{nm}(\rho_L, U) = 4\text{Re}(\text{tr}(\partial_n U \rho_L \partial_m U^\dagger) - \text{tr}(\partial_n U \rho_L U^\dagger) \text{tr}(U \rho_L \partial_m U^\dagger)) \quad (4)$$

where ∂_n is the derivative in respect to the n th entry of the M -dimensional vector $\boldsymbol{\theta} = (\theta_1, \dots, \theta_M)$.

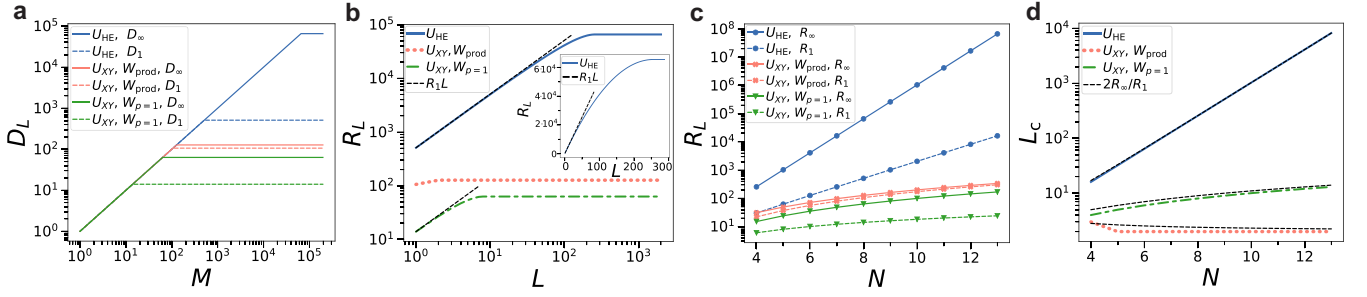


FIG. 2. DQFIM for different unitaries U with M parameters and L training states. As defined in SM D, we show hardware efficient circuit U_{HE} with no symmetries and Haar random training states (blue curves), as well as U_{XY} with particle number symmetry using as training data either product states W_{prod} (orange) or symmetry-conserving states $W_{p=1}$ (green). **a**) Effective dimension D_L increases linearly with M , until it reaches a maximal value R_L for $M \geq M_c(L)$. We have $N = 8$ qubits. **b**) R_L increases with L until converging to R_∞ for $L \geq L_c$. Black dashed line shows approximation $R_L \sim R_1 L$. Inset shows generic ansatz without log-plot, highlighting the non-linear behavior of R_L . **c**) Scaling of R_1 and R_∞ with qubit number N . **d**) Number L_c of training states needed for generalization. Black dashed line shows $L_c \approx 2R_\infty/R_1$.

In SM A, we derive $\mathcal{Q}(\rho_L, U(\theta))$ as the metric that describes how a variation $\theta \rightarrow \theta + d\theta$ changes the projection of $U(\theta)$ onto ρ_L , and relate the DQFIM to the QFIM of the purification of ρ_L . For $L = 1$, we recover the QFIM $\mathcal{F}_{nm} = 4\text{Re}(\langle \partial_n \psi | \partial_m \psi \rangle - \langle \partial_n \psi | \psi \rangle \langle \psi | \partial_m \psi \rangle)$ [60, 66].

The rank of \mathcal{Q} gives the effective dimension

$$D_L(\rho_L, U(\theta)) = \text{rank}(\mathcal{Q}(\rho_L, U(\theta))) \leq M. \quad (5)$$

The case $L = 1$ has been studied previously [49]: The effective dimension D_1 increases with M , until reaching a maximal value R_1 (see Fig. 2a). Once maximal, the parameterized state $U(\theta)|\psi_1\rangle$ is overparameterized as it can explore all its degrees of freedom [59]. Note that it is sufficient to consider a randomly chosen θ to get the generic behavior of D_1 [49]. Similarly for general L , D_L increases with M until a maximal R_L , which describes the maximal number of degrees of freedom that U_L can explore and heralds overparameterization:

Definition 3 (Overparameterization). *Ansatz $U(\theta)$ with training data ρ_L is overparameterized when effective dimension D_L does not increase further upon increasing the number of parameters M . The maximal rank R_L reached at critical number of parameters $M \geq M_c(L)$:*

$$R_L \equiv \max_{M \geq M_c(L), \theta} D_L(\rho_L, U(\theta)). \quad (6)$$

For overparameterization with $M \geq M_c(L)$, a variation of θ can explore all degrees of freedom of U_L and thus likely find the global minimum [59, 67–70]:

Observation 1 (Convergence to global minimum). *Global minimum $C_{\text{train}}(\theta^*) \approx 0$ with training set S_L is reached with high probability when $M \geq M_c(L) \geq R_L$.*

As seen in Fig. 2b, R_L increases with L , where the growth slows down due to unitary constraints. We find the tight upper bound (SM B or [73])

$$R_L \leq 2dL - L^2 - 1 \text{ for } L \leq d; \quad R_L \leq d^2 - 1 \text{ for } L > d. \quad (7)$$

R_L increases with L until its maximal possible value $R_{L_c} \equiv R_\infty$. Here, the training data is overcomplete and sufficient to learn all degrees of freedom of $U(\theta)$:

Definition 4 (Overcomplete data). *A given model $U(\theta)$ and ρ_L is overcomplete when R_L does not increase further upon increasing L . Its maximal rank $R_\infty = R_{L_c}$ is reached for a critical number of training data $L \geq L_c$*

$$R_\infty = R_{L_c} \equiv \max_{L \geq L_c} R_L(\rho_L, U). \quad (8)$$

We bound R_L similar to R_1 for Ref. [59] (see SM C):

Theorem 1. *The maximal rank R_L is bounded by the dimension of the DLA $R_L \leq \dim(\mathfrak{g})$ where $\mathfrak{g} = \text{span}\langle iH_1, \dots, iH_K \rangle_{\text{Lie}}$ is generated by the repeated nested commutators of the generators H_k of $U(\theta)$.*

Thus, using an ansatz with restricted Lie algebra [43, 45, 74] with $\dim(\mathfrak{g}) \sim \text{poly}(N)$ generalizes with $L_c, M_c \sim \text{poly}(N)$ where N is the number of qubits.

We can estimate L_c with the following consideration: To generalize we have to learn all R_∞ degrees of freedom of the unitary. The first training state allows us to learn R_1 degrees of freedom, while each additional state provides a bit less as seen in Eq. (7). For the upper bound of Eq. (7) we have $L_c \approx 2R_\infty/R_1$, which we numerically find to be a good estimator also for other models:

Observation 2 (Generalization for learning unitaries). *A trained model generalizes $C_{\text{test}}(\theta^*) \approx 0$ with high probability when the model is overparameterized (i.e. $M \geq M_c \geq R_L$ for Def. 3) and overcomplete (i.e. $L \geq L_c$ for Def. 4). The critical number of training states L_c needed to generalize can be approximated by*

$$L_c \approx 2R_\infty/R_1. \quad (9)$$

Applications.— We want to learn the unitary evolution $V_{XY} = \exp(-iH_{XY}t)$ at time t of the XY-Hamiltonian $H_{XY} = \sum_{k=1}^N (\sigma_k^x \sigma_{k+1}^x + \sigma_k^y \sigma_{k+1}^y + h_k \sigma_k^z)$,

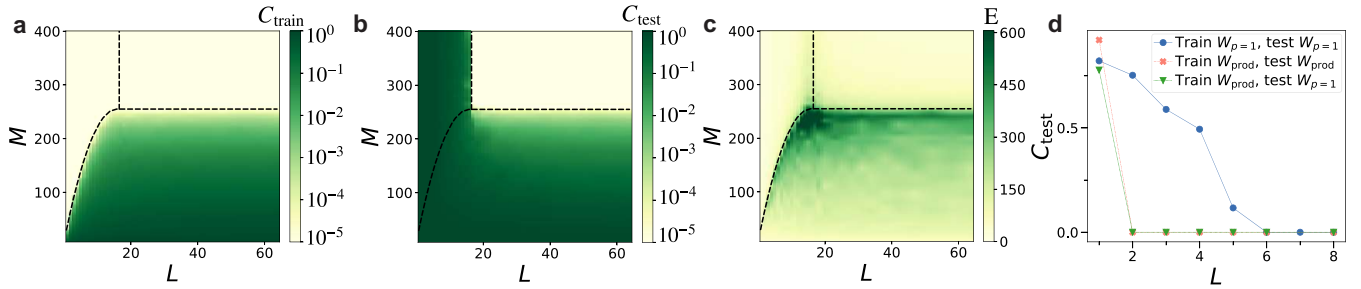


FIG. 3. **a)** Median C_{train} against M and L for learning unitaries. Dashed black lines indicate $M_c(L) = R_L$ and $L_c = 2R_\infty/R_1$. We have a $N = 4$ qubit hardware-efficient ansatz trained with random training states and gradient descent [71] simulated with [72]. Target unitary is $V = U(\theta_g)$ with random parameter θ_g , where we take median over 10 random instances. **b)** Average C_{test} against M and L . **c)** Number of training steps E until reaching $C_{\text{train}} < 10^{-4}$. **d)** C_{test} against L with particle-number conserving U_{XY} ansatz for $N = 6$ qubits and $M = 90$. We train and test with product states W_{prod} and particle-number conserving states $W_{p=1}$.

where σ_k^α , $\alpha \in \{x, y, z\}$ is the Pauli operator acting on qubit k and $h_k \in \mathbb{R}$. We learn V_{XY} with $U_{XY}(\theta)$ ansatz (see SM D for definition), which can represent any V_{XY} with polynomial number of parameters [75, 76]. H_{XY} and U_{XY} conserve the particle number operator $P = \sum_{k=1}^N \frac{1}{2}(1 - \sigma_k^z)$ with $[U_{XY}, P] = [H_{XY}, P] = 0$, where $[\cdot]$ is the commutator. We use the distribution $|\psi_\ell\rangle \in W_{p=1}$ which is symmetric in regards to P , i.e. $P|\psi_\ell\rangle = p|\psi_\ell\rangle$ with the same eigenvalue $p = 1$ for all $|\psi_\ell\rangle \in W_{p=1}$. Further, we have the single-qubit product states W_{prod} with $|\psi_\ell\rangle = \bigotimes_{k=1}^N |\phi_\ell^k\rangle$, $|\phi_\ell^k\rangle \in \mathcal{H}(\mathbb{C}^2)$ which are not symmetric in respect to P .

Observation 3 (Non-symmetric data improves generalization). *We train $U_{XY}(\theta)$ with (i) particle-number conserving states $|\psi_\ell\rangle \in W_{p=1}$ and (ii) single-qubit product states $|\psi_\ell\rangle \in W_{\text{prod}}$. For $W_{p=1}$ we find exactly $R_1 = 2N - 2$, $R_\infty = N^2 - 1$, while for W_{prod} we find via numerical extrapolation $R_1 = 2N^2 - 3N + 2$ and $R_\infty = 2N^2 - 1$ (Fig. 2c,d). Generalization requires less $L_c \approx 2R_\infty/R_1$ training states for non-symmetric data:*

- (i) *Symmetric*: $L_c = N$ for $|\psi_\ell\rangle \in W_{p=1}$
- (ii) *Non-symmetric*: $L_c = 2$ for $|\psi_\ell\rangle \in W_{\text{prod}}$, $N > 4$.

Intuitively, non-symmetric data requires less L as it can use information from other symmetry sectors.

Next, we consider out-of-distribution generalization where the training data is drawn from a different distribution than the test data [8]:

Observation 4 (Out-of-distribution generalization requires less data). *Training $U_{XY}(\theta)$ with product states $|\psi_\ell\rangle \in W_{\text{prod}}$, but testing with number-conserving data $W_{p=1}$ achieves out-of-distribution generalization with only $L \geq 2$ training data. In contrast, in-distribution training and testing with number-conserving data $|\psi_\ell\rangle \in W_{p=1}$ requires $L \geq N$ states to generalize.*

This result follows from Obs. 3 and product states being sufficient to learn arbitrary unitaries [8]. We confirm

our result numerically in Fig. 3d

Numerical results.— In Fig. 3a-c we study learning of unitaries with hardware-efficient ansatz $U_{\text{HE}}(\theta)$ (see SM D). In Fig. 3a, we converge to local minima with $C_{\text{train}} \gg 0$ for $M \leq R_L$, while we find global minimum $C_{\text{train}} \approx 0$ for $M \geq R_L$, which is indicated as black dashed line. In Fig. 3b, generalization $C_{\text{test}} \approx 0$ is achieved only for $M \geq R_\infty$ and $L \geq L_c \approx 2R_\infty/R_1$ indicated by the vertical black line. In Fig. 3c, the number of training steps E to converge show characteristic peaks close to M_c and L_c indicated by black dashed lines. In Fig. 3d we show the test error against L for the U_{XY} ansatz which conserves particle number P . We find that training with symmetric data W_{prod} generalizes for $L \geq 2$, while training with non-symmetric $W_{p=1}$ generalizes for $L \geq N$ which numerically confirms Obs. 3. Further, the green curve shows out-of-distribution generalization where training with W_{prod} generalizes with test data from $W_{p=1}$ using only $L \geq 2$, while in-distribution learning (blue curve) requires $L \geq N$, confirming Obs. 4. We study U_{XY} in more detail in SM E and other models which generalize for constant L in SM F.

Conclusion.— Our newly introduced DQFIM \mathcal{Q} and its maximal rank R_L quantify the learnable degrees of freedom of ansatz $U(\theta)$ using L training states. R_L increases with L until the training data becomes overcomplete at $R_{L_c} = R_\infty$ and $L_c \approx 2R_\infty/R_1$ where one is able to generalize.

Overparameterized models converge to global minima with high probability [59, 67, 69, 70, 77–79]. We show that overparameterization depends on L and occurs for $M \geq M_c(L) \geq R_L$ circuit parameters. Overparameterization and generalization appear in three distinct regimes, where training time increases substantially at the transitions, potentially indicating computational phase transitions [26, 69].

While symmetries have been shown to improve generalization [45, 46], we show that symmetries in data can also increase L needed to generalize due to higher

R_∞/R_1 ratio compared to non-symmetric data. This also implies that *out-of-distribution generalization can outperform in-distribution generalization* when training on non-symmetric data, but testing on symmetric data. Note that non-symmetric data has larger M_c , which implies an interesting trade-off between L_c and M_c .

The DQFIM accurately characterizes overparameterization and generalization depending on the specific structure and symmetries of ansatz $U(\theta)$ and training data ρ_L . In contrast, previously considered uniform generalization bounds provide only a loose bound on generalization error $\sim \sqrt{1/L}$ without accounting for symmetries [7, 39]. We demonstrate the relationship between DLA and generalization, showing that polynomial DLA implies overparameterization and generalization with polynomial circuit depth and dataset size. Generalization with few data is possible whenever $R_\infty/R_1 = \text{const}$, explaining the numerical observations of Ref. [10, 39] (see also SM F). Thus, problem classes with polynomial DLA [41, 74, 80] can be trained with low data cost and avoid barren plateaus [81, 82].

Our results apply to various quantum machine learning algorithms. We study unitary learning problems, which includes quantum compiling [30], quantum control (SM G), and quantum generative models (SM H). In SM I the DQFIM determines convergence of the subspace-search variational quantum eigensolver (SSVQE) for finding eigenstates of Hamiltonians [83]. In SM J we apply the DQFIM for classification tasks. Here, the label operator $O_\ell = y_\ell \sigma^z$ is not a projector and thus has not only one, but 2^{N-1} degenerate solutions. This reduces $M_c(L) \approx R_L \gamma$ by a constant factor $\gamma \leq 1$ where for a generic ansatz we find $\gamma = \frac{1}{2}$. γ can be smaller when the ansatz has symmetries which opens an interesting approach to reduce circuit depth in classification tasks.

Numerical evaluation of the DQFIM is straightforward via differentiation (with code available online [84]) and is scalable for matrix product states. Quantum computers can efficiently measure the DQFIM using the Hadamard test with a single ancilla and two control operations, or alternatively the shift-rule and purification [85] in SM A.

While the complexity of unitaries grows linearly with M [49, 86], we find that the learnable degrees of freedom R_L of unitaries grows only sub-linearly with L . Generalization error for overparameterized models scales as $C_{\text{test}} \sim 1 - (L/L_c)^2$ (see SM E) which saturates the lower bound derived in Ref. [6]. We note that for underparameterized models the empirical generalization error $C_{\text{test}} - C_{\text{train}}$ [40] is not a good indicator of generalization due to convergence to bad local minima (see SM K).

Finally, future work can apply the DQFIM for data re-uploading [87, 88], kernel models [89, 90], noisy systems [61] and quantum natural gradients [91].

Acknowledgements— We thank Adithya Sireesh and Raghavendra Peddinti for discussions. This work is sup-

ported by a Samsung GRC project and the UK Hub in Quantum Computing and Simulation, part of the UK National Quantum Technologies Programme with funding from UKRI EPSRC grant EP/T001062/1.

* tobias.haug@u.nus.edu

- [1] J. Biamonte, P. Wittek, N. Pancotti, P. Rebentrost, N. Wiebe, and S. Lloyd, Quantum machine learning, *Nature* **549**, 195 (2017).
- [2] K. Poland, K. Beer, and T. J. Osborne, No free lunch for quantum machine learning, arXiv:2003.14103 (2020).
- [3] M. C. Caro and I. Datta, Pseudo-dimension of quantum circuits, *Quantum Machine Intelligence* **2**, 14 (2020).
- [4] A. Abbas, D. Sutter, C. Zoufal, A. Lucchi, A. Figalli, and S. Woerner, The power of quantum neural networks, *Nature Computational Science* **1**, 403 (2021).
- [5] A. Abbas, D. Sutter, A. Figalli, and S. Woerner, Effective dimension of machine learning models, arXiv:2112.04807 (2021).
- [6] K. Sharma, M. Cerezo, Z. Holmes, L. Cincio, A. Sornborger, and P. J. Coles, Reformulation of the no-free-lunch theorem for entangled datasets, *Physical Review Letters* **128**, 070501 (2022).
- [7] L. Banchi, J. Pereira, and S. Pirandola, Generalization in quantum machine learning: A quantum information standpoint, *PRX Quantum* **2**, 040321 (2021).
- [8] M. C. Caro, H.-Y. Huang, N. Ezzell, J. Gibbs, A. T. Sornborger, L. Cincio, P. J. Coles, and Z. Holmes, Out-of-distribution generalization for learning quantum dynamics, *Nature Communications* **14**, 3751 (2023).
- [9] E. Peters and M. Schuld, Generalization despite overfitting in quantum machine learning models, *Quantum* **7**, 1210 (2023).
- [10] J. Gibbs, Z. Holmes, M. C. Caro, N. Ezzell, H.-Y. Huang, L. Cincio, A. T. Sornborger, and P. J. Coles, Dynamical simulation via quantum machine learning with provable generalization, *Physical Review Research* **6**, 013241 (2024).
- [11] T. Volkoff, Z. Holmes, and A. Sornborger, Universal compiling and (no-) free-lunch theorems for continuous-variable quantum learning, *PRX Quantum* **2**, 040327 (2021).
- [12] H. Cai, Q. Ye, and D.-L. Deng, Sample complexity of learning parametric quantum circuits, *Quantum Science and Technology* **7**, 025014 (2022).
- [13] C. M. Popescu, Learning bounds for quantum circuits in the agnostic setting, *Quantum Information Processing* **20**, 286 (2021).
- [14] M. C. Caro, E. Gil-Fuster, J. J. Meyer, J. Eisert, and R. Sweke, Encoding-dependent generalization bounds for parametrized quantum circuits, *Quantum* **5**, 582 (2021).
- [15] K. Bu, D. E. Koh, L. Li, Q. Luo, and Y. Zhang, Statistical complexity of quantum circuits, *Physical Review A* **105**, 062431 (2022).
- [16] J. Bowles, V. J. Wright, M. Farkas, N. Killoran, and M. Schuld, Contextuality and inductive bias in quantum machine learning, arXiv:2302.01365 (2023).
- [17] Y. Du, Y. Yang, D. Tao, and M.-H. Hsieh, Demystify problem-dependent power of quantum neural networks on multi-class classification, arXiv:2301.01597 (2022).

- [18] K. Bu, D. E. Koh, L. Li, Q. Luo, and Y. Zhang, Effects of quantum resources and noise on the statistical complexity of quantum circuits, *Quantum Science and Technology* **8**, 025013 (2023).
- [19] K. Gili, M. Mauri, and A. Perdomo-Ortiz, Evaluating generalization in classical and quantum generative models, arXiv:2201.08770 (2022).
- [20] A. Bisio, G. Chiribella, G. M. D'Ariano, S. Facchini, and P. Perinotti, Optimal quantum learning of a unitary transformation, *Physical Review A* **81**, 032324 (2010).
- [21] I. Marvian and S. Lloyd, Universal quantum emulator, arXiv preprint arXiv:1606.02734 (2016).
- [22] K. Bharti, A. Cervera-Lierta, T. H. Kyaw, T. Haug, S. Alperin-Lea, A. Anand, M. Degroote, H. Heimonen, J. S. Kottmann, T. Menke, W.-K. Mok, S. Sim, L.-C. Kwek, and A. Aspuru-Guzik, Noisy intermediate-scale quantum algorithms, *Rev. Mod. Phys.* **94**, 015004 (2022).
- [23] M. Cerezo, A. Arrasmith, R. Babbush, S. C. Benjamin, S. Endo, K. Fujii, J. R. McClean, K. Mitarai, X. Yuan, L. Cincio, *et al.*, Variational quantum algorithms, *Nature Reviews Physics* **3**, 625 (2021).
- [24] S. Xue, Y. Liu, Y. Wang, P. Zhu, C. Guo, and J. Wu, Variational quantum process tomography of unitaries, *Physical Review A* **105**, 032427 (2022).
- [25] V. Gebhart, R. Santagati, A. A. Gentile, E. M. Gauger, D. Craig, N. Ares, L. Banchi, F. Marquardt, L. Pezzè, and C. Bonato, Learning quantum systems, *Nature Reviews Physics* , 1 (2023).
- [26] B. T. Kiani, S. Lloyd, and R. Maity, Learning unitaries by gradient descent, arXiv:2001.11897 (2020).
- [27] Z. Yu, X. Zhao, B. Zhao, and X. Wang, Optimal quantum dataset for learning a unitary transformation, *Physical Review Applied* **19**, 034017 (2023).
- [28] E. Farhi and H. Neven, Classification with quantum neural networks on near term processors, arXiv:1802.06002 (2018).
- [29] M. Schuld, A. Bocharov, K. M. Svore, and N. Wiebe, Circuit-centric quantum classifiers, *Physical Review A* **101**, 032308 (2020).
- [30] S. Khatri, R. LaRose, A. Poremba, L. Cincio, A. T. Sornborger, and P. J. Coles, Quantum-assisted quantum compiling, *Quantum* **3**, 140 (2019).
- [31] N. Ezzell, E. M. Ball, A. U. Siddiqui, M. M. Wilde, A. T. Sornborger, P. J. Coles, and Z. Holmes, Quantum mixed state compiling, *Quantum Sci. Technol.* **8**, 10.1088/2058-9565/acc4e3 (2023).
- [32] B. Coyle, D. Mills, V. Danos, and E. Kashefi, The born supremacy: quantum advantage and training of an ising born machine, *npj Quantum Information* **6**, 60 (2020).
- [33] K. Gili, M. Hibat-Allah, M. Mauri, C. Ballance, and A. Perdomo-Ortiz, Do quantum circuit born machines generalize?, *Quantum Science and Technology* **8**, 035021 (2023).
- [34] C. Cirstoiu, Z. Holmes, J. Iosue, L. Cincio, P. J. Coles, and A. Sornborger, Variational fast forwarding for quantum simulation beyond the coherence time, *npj Quantum Information* **6**, 82 (2020).
- [35] J. Gibbs, K. Gili, Z. Holmes, B. Commeau, A. Arrasmith, L. Cincio, P. J. Coles, and A. Sornborger, Long-time simulations for fixed input states on quantum hardware, *npj Quantum Information* **8**, 135 (2022).
- [36] J. Romero, J. P. Olson, and A. Aspuru-Guzik, Quantum autoencoders for efficient compression of quantum data, *Quantum Sci. Technol.* **2**, 045001 (2017).
- [37] H. Zhang, L. Wan, T. Haug, W.-K. Mok, S. Paesani, Y. Shi, H. Cai, L. K. Chin, M. F. Karim, L. Xiao, *et al.*, Resource-efficient high-dimensional subspace teleportation with a quantum autoencoder, *Science Advances* **8**, eabn9783 (2022).
- [38] L. Leone, S. F. Oliviero, S. Piemontese, S. True, and A. Hamma, Retrieving information from a black hole using quantum machine learning, *Physical Review A* **106**, 062434 (2022).
- [39] M. C. Caro, H.-Y. Huang, M. Cerezo, K. Sharma, A. Sornborger, L. Cincio, and P. J. Coles, Generalization in quantum machine learning from few training data, *Nature communications* **13**, 4919 (2022).
- [40] E. Gil-Fuster, J. Eisert, and C. Bravo-Prieto, Understanding quantum machine learning also requires rethinking generalization, *Nature Communications* **15**, 1 (2024).
- [41] L. Schatzki, M. Larocca, Q. T. Nguyen, F. Sauvage, and M. Cerezo, Theoretical guarantees for permutation-equivariant quantum neural networks, *npj Quantum Information* **10**, 12 (2024).
- [42] M. Ragone, P. Braccia, Q. T. Nguyen, L. Schatzki, P. J. Coles, F. Sauvage, M. Larocca, and M. Cerezo, Representation theory for geometric quantum machine learning, arXiv:2210.07980 (2022).
- [43] Q. T. Nguyen, L. Schatzki, P. Braccia, M. Ragone, P. J. Coles, F. Sauvage, M. Larocca, and M. Cerezo, Theory for equivariant quantum neural networks, arXiv:2210.08566 (2022).
- [44] H. Zheng, Z. Li, J. Liu, S. Strelchuk, and R. Kondor, Speeding up learning quantum states through group equivariant convolutional quantum ansätze, arXiv:2112.07611 (2021).
- [45] J. J. Meyer, M. Mularski, E. Gil-Fuster, A. A. Mele, F. Arzani, A. Wilms, and J. Eisert, Exploiting symmetry in variational quantum machine learning, *PRX Quantum* **4**, 010328 (2023).
- [46] M. Larocca, F. Sauvage, F. M. Sbahi, G. Verdon, P. J. Coles, and M. Cerezo, Group-invariant quantum machine learning, *PRX Quantum* **3**, 030341 (2022).
- [47] F. Sauvage, M. Larocca, P. J. Coles, and M. Cerezo, Building spatial symmetries into parameterized quantum circuits for faster training, *Quantum Science and Technology* **9** (2024).
- [48] A. Skolik, M. Cattelan, S. Yarkoni, T. Bäck, and V. Dunjko, Equivariant quantum circuits for learning on weighted graphs, arXiv preprint arXiv:2205.06109 (2022).
- [49] T. Haug, K. Bharti, and M. Kim, Capacity and quantum geometry of parametrized quantum circuits, *PRX Quantum* **2**, 040309 (2021).
- [50] K. Bu, D. E. Koh, L. Li, Q. Luo, and Y. Zhang, Rademacher complexity of noisy quantum circuits, arXiv preprint arXiv:2103.03139 (2021).
- [51] E. R. Anschuetz, A. Bauer, B. T. Kiani, and S. Lloyd, Efficient classical algorithms for simulating symmetric quantum systems, *Quantum* **7**, 1189 (2023).
- [52] H.-Y. Huang, M. Broughton, M. Mohseni, R. Babbush, S. Boixo, H. Neven, and J. R. McClean, Power of data in quantum machine learning, *Nature communications* **12**, 1 (2021).
- [53] Y. Liu, S. Arunachalam, and K. Temme, A rigorous and robust quantum speed-up in supervised machine learning, *Nature Physics* , 1 (2021).

- [54] H.-Y. Huang, R. Kueng, G. Torlai, V. V. Albert, and J. Preskill, Provably efficient machine learning for quantum many-body problems, *Science* **377**, eabk3333 (2022).
- [55] J. Liu, M. Liu, J.-P. Liu, Z. Ye, Y. Alexeev, J. Eisert, and L. Jiang, Towards provably efficient quantum algorithms for large-scale machine-learning models, arXiv:2303.03428 (2023).
- [56] P. L. Bartlett, D. J. Foster, and M. J. Telgarsky, Spectrally-normalized margin bounds for neural networks, *Advances in neural information processing systems* **30** (2017).
- [57] Y. Jiang, B. Neyshabur, H. Mobahi, D. Krishnan, and S. Bengio, Fantastic generalization measures and where to find them, arXiv:1912.02178 (2019).
- [58] T. Liang, T. Poggio, A. Rakhlin, and J. Stokes, Fisher-rao metric, geometry, and complexity of neural networks, in *The 22nd international conference on artificial intelligence and statistics* (PMLR, 2019) pp. 888–896.
- [59] M. Larocca, N. Ju, D. García-Martín, P. J. Coles, and M. Cerezo, Theory of overparametrization in quantum neural networks, *Nature Computational Science* **3**, 542 (2023).
- [60] J. J. Meyer, Fisher information in noisy intermediate-scale quantum applications, *Quantum* **5**, 539 (2021).
- [61] D. García-Martín, M. Larocca, and M. Cerezo, Effects of noise on the overparametrization of quantum neural networks, *Physical Review Research* **6**, 013295 (2024).
- [62] R. Chakrabarti and H. Rabitz, Quantum control landscapes, *International Reviews in Physical Chemistry* **26**, 671 (2007).
- [63] M. S. Rudolph, S. Lerch, S. Thanasilp, O. Kiss, S. Vallecorsa, M. Grossi, and Z. Holmes, Trainability barriers and opportunities in quantum generative modeling, arXiv:2305.02881 (2023).
- [64] K. Mitarai, M. Negoro, M. Kitagawa, and K. Fujii, Quantum circuit learning, *Physical Review A* **98**, 032309 (2018).
- [65] M. A. Nielsen and I. Chuang, *Quantum computation and quantum information* (2002).
- [66] J. Liu, H. Yuan, X.-M. Lu, and X. Wang, Quantum fisher information matrix and multiparameter estimation, *Journal of Physics A: Mathematical and Theoretical* **53**, 023001 (2020).
- [67] H. A. Rabitz, M. M. Hsieh, and C. M. Rosenthal, Quantum optimally controlled transition landscapes, *Science* **303**, 1998 (2004).
- [68] M. Bukov, A. G. R. Day, D. Sels, P. Weinberg, A. Polkovnikov, and P. Mehta, Reinforcement learning in different phases of quantum control, *Phys. Rev. X* **8**, 031086 (2018).
- [69] E. R. Anschuetz, Critical points in quantum generative models, arXiv:2109.06957 (2021).
- [70] X. You, S. Chakrabarti, and X. Wu, A convergence theory for over-parameterized variational quantum eigensolvers, arXiv:2205.12481 (2022).
- [71] R. Fletcher, *Practical methods of optimization* (John Wiley & Sons, 2013).
- [72] J. R. Johansson, P. D. Nation, and F. Nori, Qutip: An open-source python framework for the dynamics of open quantum systems, *Computer Physics Communications* **183**, 1760 (2012).
- [73] J. Polcari, *Representing unitary matrices by independent parameters*, Tech. Rep. (Working Paper, Rev 0, October, 2016, 2016).
- [74] R. Wiersema, E. Kökcü, A. F. Kemper, and B. N. Bakalov, Classification of dynamical lie algebras for translation-invariant 2-local spin systems in one dimension, arXiv:2309.05690 (2023).
- [75] E. Kökcü, D. Camps, L. B. Oftelie, J. K. Freericks, W. A. de Jong, R. Van Beeumen, and A. F. Kemper, Algebraic compression of quantum circuits for hamiltonian evolution, *Physical Review A* **105**, 032420 (2022).
- [76] E. Kökcü, T. Steckmann, Y. Wang, J. Freericks, E. F. Dumitrescu, and A. F. Kemper, Fixed depth hamiltonian simulation via cartan decomposition, *Physical Review Letters* **129**, 070501 (2022).
- [77] J. Kim, J. Kim, and D. Rosa, Universal effectiveness of high-depth circuits in variational eigenproblems, *Physical Review Research* **3**, 023203 (2021).
- [78] E. Campos, A. Nasrallah, and J. Biamonte, Abrupt transitions in variational quantum circuit training, *Physical Review A* **103**, 032607 (2021).
- [79] J. Kim and Y. Oz, Quantum energy landscape and circuit optimization, *Physical Review A* **106**, 052424 (2022).
- [80] F. Sauvage, M. Larocca, P. J. Coles, and M. Cerezo, Building spatial symmetries into parameterized quantum circuits for faster training, *Quantum Science and Technology* **9**, 015029 (2024).
- [81] E. Fontana, D. Herman, S. Chakrabarti, N. Kumar, R. Yalovetzky, J. Heredge, S. H. Sureshbabu, and M. Pistoia, The adjoint is all you need: Characterizing barren plateaus in quantum ansatz, arXiv:2309.07902 (2023).
- [82] M. Ragone, B. N. Bakalov, F. Sauvage, A. F. Kemper, C. O. Marrero, M. Larocca, and M. Cerezo, A unified theory of barren plateaus for deep parametrized quantum circuits, arXiv:2309.09342 (2023).
- [83] K. M. Nakanishi, K. Mitarai, and K. Fujii, Subspace-search variational quantum eigensolver for excited states, *Physical Review Research* **1**, 033062 (2019).
- [84] T. Haug, Generalization with quantum geometry, https://github.com/txhaug/geometric_generalization.
- [85] A. Mari, T. R. Bromley, and N. Killoran, Estimating the gradient and higher-order derivatives on quantum hardware, *Physical Review A* **103**, 012405 (2021).
- [86] J. Haferkamp, P. Faist, N. B. Kothakonda, J. Eisert, and N. Younger Halpern, Linear growth of quantum circuit complexity, *Nature Physics* **18**, 528 (2022).
- [87] A. Pérez-Salinas, A. Cervera-Lierta, E. Gil-Fuster, and J. I. Latorre, Data re-uploading for a universal quantum classifier, *Quantum* **4**, 226 (2020).
- [88] S. Jerbi, L. J. Fiderer, H. Poulsen Nautrup, J. M. Kübler, H. J. Briegel, and V. Dunjko, Quantum machine learning beyond kernel methods, *Nature Communications* **14**, 517 (2023).
- [89] M. Schuld and N. Killoran, Quantum machine learning in feature hilbert spaces, *Physical review letters* **122**, 040504 (2019).
- [90] T. Haug, C. N. Self, and M. S. Kim, Quantum machine learning of large datasets using randomized measurements, *Machine Learning: Science and Technology* **4**, 015005 (2023).
- [91] J. Stokes, J. Izaac, N. Killoran, and G. Carleo, Quantum natural gradient, *Quantum* **4**, 269 (2020).
- [92] R. Cheng, Quantum geometric tensor (fubini-study metric) in simple quantum system: A pedagogical introduction, arXiv:1012.1337 (2010).
- [93] Y. Li and S. C. Benjamin, Efficient variational quantum

- simulator incorporating active error minimization, Physical Review X **7**, 021050 (2017).
- [94] X. Yuan, S. Endo, Q. Zhao, Y. Li, and S. C. Benjamin, Theory of variational quantum simulation, Quantum **3**, 191 (2019).
- [95] D. d'Alessandro, *Introduction to quantum control and dynamics* (Chapman and hall/CRC, 2021).
- [96] J. Werschnik and E. Gross, Quantum optimal control theory, Journal of Physics B: Atomic, Molecular and Optical Physics **40**, R175 (2007).
- [97] N. Khaneja, T. Reiss, C. Kehlet, T. Schulte-Herbrüggen, and S. J. Glaser, Optimal control of coupled spin dynamics: design of nmr pulse sequences by gradient ascent algorithms, Journal of magnetic resonance **172**, 296 (2005).
- [98] K. Bharti, T. Haug, V. Vedral, and L.-C. Kwek, Nisq algorithm for semidefinite programming, arXiv:2106.03891 (2021).

Supplemental Material

In the Supplemental Material, we derive the data quantum Fisher information metric (DQFIM) from first principles, connect it to the purification of the quantum Fisher information metric, and show how to measure the DQFIM on quantum computers. We prove that the dynamical Lie algebra bounds the DQFIM. Further, we define the ansatz unitaries used in the main text and study the DQFIM with other types of variational ansatz. Finally, we use the DQFIM to study overparameterization and generalization for various quantum machine learning models, such as quantum control, generative models, finding eigenstates of Hamiltonians and classification tasks.

Contents

A. Data quantum Fisher information (DQFIM)	9
1. Recap of quantum Fisher information metric	9
2. Derivation of DQFIM	10
3. DQFIM as purification of QFIM	12
4. Measuring DQFIM on quantum computers using Hadamard test	12
5. Measuring DQFIM on quantum computers using shift-rule and purification	13
B. Degrees of freedom of isometries	14
C. Lie-algebra bound on the rank of DQFIM	15
D. Ansatz unitaries	16
E. Additional results on XY circuit learning	17
F. Generalization with further circuit models	19
G. DQFIM for overparameterization and generalization for quantum control	20
H. Overparameterization for generative models	22
I. Overparameterization of variational quantum eigensolver for eigenstates	22
J. Overparameterization and generalization in classification tasks	24
K. Generalization and empirical generalization error	25

Supplemental Materials A: Data quantum Fisher information (DQFIM)

Here, we derive our data quantum Fisher information (DQFIM) from first principles. First, we review the quantum Fisher information (QFIM). Then, we derive the DQFIM using two different approaches: First, as metric of unitary evolution projected on training data, and second as the QFIM of the purification. Finally, we show how to compute the DQFIM using two methods: Either by using the Hadamard test using one ancilla and two controlled operations, or by using the shift-rule on the purification.

1. Recap of quantum Fisher information metric

The Quantum Fisher information metric (QFIM) [60, 66] is an essential tool for quantum sensing, parameter estimation and optimization of quantum circuits. Here, we review the derivation of the QFIM or Fubini-Study metric \mathcal{F} [92]. We have a parameterized quantum state $|\psi(\boldsymbol{\theta})\rangle$. We now study the variation

$$ds^2 = |||\psi(\boldsymbol{\theta} + d\boldsymbol{\theta}) - |\psi(\boldsymbol{\theta})\rangle|| = \langle \delta\psi | \delta\psi \rangle = \langle \partial_n \psi | \partial_m \psi \rangle d\boldsymbol{\theta}^n d\boldsymbol{\theta}^m = (\gamma_{nm} + i\sigma_{nm}) d\boldsymbol{\theta}^n d\boldsymbol{\theta}^m$$

where we defined the real and imaginary part γ_{nm} and σ_{nm} of $\langle \partial_n \psi | \partial_m \psi \rangle$. As ds^2 is hermitian, we have $\gamma_{nm} = \gamma_{mn}$ and $\sigma_{nm} = -\sigma_{mn}$, such that $\sigma_{nm} d\theta^n d\theta^m$ vanishes. However, γ_{nm} is not a proper metric as it is not invariant under the gauge transformation $|\psi'\rangle = \exp(i\alpha)|\psi\rangle$ under a global phase rotation with α . We now construct a proper gauge invariant metric.

First, one can easily show by using $\langle \psi | \psi \rangle = 1$ that $\beta_n = i\langle \psi | \partial_n \psi \rangle \in \mathbb{R}$. Next, we compute $\langle \psi' | \psi' \rangle = \gamma'_{nm} + i\sigma'_{nm}$, where a straightforward calculation yields

$$\gamma'_{nm} = \gamma_{nm} + \partial_n \alpha \partial_m \alpha - \beta_m \gamma_n \alpha - \beta_n \gamma_m \alpha \quad (\text{S1})$$

and $\sigma'_{nm} = \sigma_{nm}$. From this result, we now define a gauge-invariant metric

$$g_{nm} = \gamma_{nm} - \beta_n \beta_m \quad (\text{S2})$$

where one can easily confirm $g'_{nm} = g_{nm}$ by using $\beta'_n = \beta_n - \partial_n \alpha$. We can think of γ_{nm} measuring the change of $|\psi(\boldsymbol{\theta})\rangle$ in the Hilbertspace, while g_{nm} measures its change excluding global phases which have no observable effect.

The quantum geometric tensor is defined as

$$\Xi_{nm} = \langle \partial_n \psi | \partial_m \psi \rangle - \langle \partial_n \psi | \psi \rangle \langle \psi | \partial_m \psi \rangle \quad (\text{S3})$$

and the QFIM as $\mathcal{F}_{nm} = 4\text{Re}(\Xi_{nm})$, which corresponds to the real part of g_{nm} .

The QFIM describes the change in fidelity for $|\langle \psi(\boldsymbol{\theta}) | \psi(\boldsymbol{\theta} + d\boldsymbol{\theta}) \rangle|^2$ as we will see in the following. First, note that $\langle \psi | \partial_n \psi \rangle \in \text{Im}$. Thus, its derivative must be also imaginary, i.e. $\langle \psi | \partial_n \partial_m \psi \rangle + \langle \partial_m \psi | \partial_n \psi \rangle \in \text{Im}$, which immediately implies

$$\langle \psi | \partial_n \partial_m \psi \rangle = -\langle \partial_m \psi | \partial_n \psi \rangle. \quad (\text{S4})$$

Now, we find via Taylor expansion

$$\begin{aligned} \langle \psi(\boldsymbol{\theta}) | \psi(\boldsymbol{\theta} + d\boldsymbol{\theta}) \rangle &\approx \\ 1 + i\langle \psi | \partial_n \psi \rangle d\theta^n + \frac{1}{2}\langle \psi | \partial_n \partial_m \psi \rangle d\theta^n d\theta^m &= \\ 1 + i\langle \psi | \partial_n \psi \rangle d\theta^n - \frac{1}{2}\langle \partial_n \psi | \partial_m \psi \rangle d\theta^n d\theta^m & \end{aligned} \quad (\text{S5})$$

Now, we compute using Eq. (S5)

$$\begin{aligned} |\langle \psi(\boldsymbol{\theta}) | \psi(\boldsymbol{\theta} + d\boldsymbol{\theta}) \rangle|^2 &= \\ \langle \psi(\boldsymbol{\theta}) | \psi(\boldsymbol{\theta} + d\boldsymbol{\theta}) \rangle \langle \psi(\boldsymbol{\theta} + d\boldsymbol{\theta}) | \psi(\boldsymbol{\theta}) \rangle &\approx \\ 1 - [\langle \partial_n \psi | \psi \rangle \langle \psi | \partial_m \psi \rangle] & \\ + \frac{1}{2}\langle \partial_n \psi | \partial_m \psi \rangle + \frac{1}{2}\langle \partial_m \psi | \partial_n \psi \rangle] d\theta^n d\theta^m &= \\ 1 - \text{Re}[\langle \partial_n \psi | \partial_m \psi \rangle - \langle \partial_n \psi | \psi \rangle \langle \psi | \partial_m \psi \rangle] d\theta^n d\theta^m. & \end{aligned}$$

where in the second step we used Eq. (S4). Finally, we have

$$|\langle \psi(\boldsymbol{\theta}) | \psi(\boldsymbol{\theta} + d\boldsymbol{\theta}) \rangle|^2 = 1 - \frac{1}{4}\mathcal{F}_{nm} d\theta^n d\theta^m. \quad (\text{S6})$$

This implies that \mathcal{F} is a metric that describes the change in state space under a variation in parameter $\boldsymbol{\theta}$.

2. Derivation of DQFIM

We now generalize the QFIM to the DQFIM, which describes learning with L training states. We have a training set $S_L = \{|\psi_\ell\rangle, O_\ell\}_{\ell=1}^L$ and an ansatz $U(\boldsymbol{\theta}) \equiv U$. We recall the datastate

$$\rho_L = L^{-1} \sum_{\ell=1}^L |\psi_\ell\rangle \langle \psi_\ell| \quad (\text{S7})$$

which is the mixture of all training states.

We now derive the DQFIM Eq. (S11) from a variational principle in a similar manner as the QFIM. We consider $U(\boldsymbol{\theta})$ mapped onto the subspace of the datastate ρ_L written as $U(\boldsymbol{\theta})\rho_L$. The degrees of freedom of $U(\boldsymbol{\theta})\rho_L$ describe the degrees of freedom that can be learned about $U(\boldsymbol{\theta})$ using the training dataset.

We now have

$$\begin{aligned} ds^2 &= \|(U(\boldsymbol{\theta} + d\boldsymbol{\theta}) - U(\boldsymbol{\theta}))\sqrt{\rho_L}\|/\beta = \text{tr}(\delta U \rho_L \delta U^\dagger) = \\ &\text{tr}(\partial_n U \rho_L \partial_m U^\dagger) d\boldsymbol{\theta}^n d\boldsymbol{\theta}^m = (\gamma_{nm} + i\sigma_{nm}) d\boldsymbol{\theta}^n d\boldsymbol{\theta}^m, \end{aligned}$$

where we have the difference $\delta U = U(\boldsymbol{\theta} + d\boldsymbol{\theta}) - U(\boldsymbol{\theta})$, the square of the Frobenius norm $\|A\| = \text{tr}(A^\dagger A)$, the real and imaginary part γ_{nm} and σ_{nm} of $\text{tr}(\partial_n U \rho_L \partial_m U^\dagger)$. Note that we have $\text{tr}(U \rho_L U^\dagger) = 1$. One can now immediately check that one recovers the regular QFIM for $\rho_1 = |\psi\rangle\langle\psi|$. As ds^2 is hermitian, we have $\gamma_{nm} = \gamma_{mn}$ and $\sigma_{nm} = -\sigma_{mn}$, such that $\sigma_{nm} d\boldsymbol{\theta}^n d\boldsymbol{\theta}^m$ vanishes. However, γ_{nm} is not a proper metric as it is not invariant under the gauge transformation $U' = \exp(i\alpha)U$, i.e. a global phase rotation with α . We now construct a proper gauge invariant metric.

First, we apply ∂_n to $\text{tr}(U \rho_L U^\dagger) = 1$ and see that $\text{tr}(\partial_n U \rho_L U^\dagger) + \text{tr}(U \rho_L \partial_n U^\dagger) = 0$. It follows that $\text{tr}(U \rho_L \partial_n U^\dagger) + \text{tr}(U \rho_L \partial_n U^\dagger)^\dagger = 0$ and thus $\beta_n = i \text{tr}(U \rho_L \partial_n U^\dagger) \in \mathbb{R}$. Next, we compute $\text{tr}(U' \rho_L U'^\dagger) = \gamma'_{nm} + i\sigma'_{nm}$, where a straightforward calculation yields

$$\gamma'_{nm} = \gamma_{nm} + \partial_n \alpha \partial_m \alpha - \beta_n \gamma_n \alpha - \beta_n \gamma_m \quad (\text{S8})$$

and $\sigma'_{nm} = \sigma_{nm}$. From this result, we now define a gauge-invariant metric

$$g_{nm} = \gamma_{nm} - \beta_n \beta_m \quad (\text{S9})$$

where one can easily confirm $g'_{nm} = g_{nm}$ by using $\beta'_n = \beta_n - \partial_n \alpha$. We can think of γ_{nm} measuring the change of $U(\boldsymbol{\theta})\rho_L$ in the full isometric space, while g_{nm} measures the change excluding global phases which have no observable effect.

In analogy to the quantum geometric tensor, we define the data quantum geometric tensor

$$\Xi_{nm} = \text{tr}(\partial_n U \rho_L \partial_m U^\dagger) - \text{tr}(\partial_n U \rho_L U^\dagger) \text{tr}(U \rho_L \partial_m U^\dagger) \quad (\text{S10})$$

and the DQFIM as $\mathcal{Q}_{nm} = 4\text{Re}(\Xi_{nm})$, which corresponds to the real part of g_{nm} , with

$$\mathcal{Q}_{nm}(\rho_L) = 4\text{Re}(\text{tr}(\partial_n U \rho_L \partial_m U^\dagger) - \text{tr}(\partial_n U \rho_L U^\dagger) \text{tr}(U \rho_L \partial_m U^\dagger)). \quad (\text{S11})$$

Indeed, we find for $L = 1$ that $\mathcal{Q}(\rho_1) = \mathcal{F}$. In contrast, for a training set with $\rho_L = I/d$, we find what we call the unitary QFIM

$$\mathcal{Q}_{nm}^I \equiv \mathcal{Q}_{nm}(I/d) = 4\text{Re}(d^{-1} \text{tr}(\partial_n U \partial_m U^\dagger) - d^{-2} \text{tr}(\partial_n U U^\dagger) \text{tr}(U \partial_m U^\dagger)). \quad (\text{S12})$$

The DQFIM describes the change of $|\text{tr}(U(\boldsymbol{\theta})\rho_L U^\dagger(\boldsymbol{\theta} + d\boldsymbol{\theta}))|^2$ which we are going to show in the following. First, note that $\text{tr}(U \rho_L \partial_n U^\dagger) \in \text{Im}$. Thus, its derivative must be also imaginary, i.e. $\text{tr}(U \rho_L \partial_n \partial_m U^\dagger) + \text{tr}(\partial_n U \rho_L \partial_m U^\dagger) \in \text{Im}$, which immediately implies

$$\text{tr}(U \rho_L \partial_n \partial_m U^\dagger) = -\text{tr}(\partial_n U \rho_L \partial_m U^\dagger). \quad (\text{S13})$$

Now, we find via Taylor expansion

$$\begin{aligned} \text{tr}(U(\boldsymbol{\theta})\rho_L U(\boldsymbol{\theta} + d\boldsymbol{\theta})^\dagger) &\approx \\ 1 + i \text{tr}(U \rho_L \partial_n U^\dagger) d\boldsymbol{\theta}^n + \frac{1}{2} \text{tr}(U \rho_L \partial_n \partial_m U^\dagger) d\boldsymbol{\theta}^n d\boldsymbol{\theta}^m &= \\ 1 + i \text{tr}(U \rho_L \partial_n U^\dagger) d\boldsymbol{\theta}^n - \frac{1}{2} \text{tr}(\partial_n U \rho_L \partial_m U^\dagger) d\boldsymbol{\theta}^n d\boldsymbol{\theta}^m & \end{aligned} \quad (\text{S14})$$

Now, we compute using Eq. (S14)

$$\begin{aligned} |\text{tr}(U(\boldsymbol{\theta})\rho_L U(\boldsymbol{\theta} + d\boldsymbol{\theta})^\dagger)|^2 &= \\ \text{tr}(U(\boldsymbol{\theta})\rho_L U(\boldsymbol{\theta} + d\boldsymbol{\theta})^\dagger) \text{tr}(U(\boldsymbol{\theta} + d\boldsymbol{\theta}) U(\boldsymbol{\theta})^\dagger) &\approx \end{aligned}$$

$$\begin{aligned}
& 1 - [\text{tr}(\partial_n U \rho_L U^\dagger) \text{tr}(U \rho_L \partial_m U^\dagger) \\
& + \frac{1}{2} \text{tr}(\partial_n U \rho_L \partial_m U^\dagger) + \frac{1}{2} \text{tr}(\partial_m U \rho_L \partial_n U^\dagger)] d\theta^n d\theta^m = \\
& 1 - \text{Re}[\text{tr}(\partial_n U \rho_L \partial_m U^\dagger) - \\
& \text{tr}(\partial_n U \rho_L U^\dagger) \text{tr}(U \partial_m \rho_L U^\dagger)] d\theta^n d\theta^m.
\end{aligned}$$

where in the second step we used Eq. (S13). Finally, we have

$$|\text{tr}(U(\boldsymbol{\theta}) \rho_L U(\boldsymbol{\theta} + d\boldsymbol{\theta})^\dagger)|^2 = 1 - \frac{1}{4} \mathcal{Q}_{nm} d\theta^n d\theta^m, \quad (\text{S15})$$

which relates a change in parameter $\boldsymbol{\theta}$ to the change in the unitary projected onto the training states.

Note that equivalently one could also consider the projector onto the training data $\Pi_L = \sum_{k=1}^{B_L} |\phi_k\rangle\langle\phi_k|$ where $|\phi_k\rangle$ are the eigenvectors with non-zero eigenvalue of and $B_L = \text{rank}(\rho_L)$ to get the isometry $U(\boldsymbol{\theta})\Pi_L$. The rank of the DQFIM using Π_L is equivalent to the one with ρ_L .

3. DQFIM as purification of QFIM

We now show an alternative derivation of the DQFIM as the QFIM of the purification of the dataset.

The DQFIM is equivalent to the QFIM of the purification of the data state $\rho_L = \frac{1}{L} \sum_{i=1}^L |\psi_i\rangle\langle\psi_i|$. In particular, the purification $|\chi_L\rangle$ of ρ_L can be written as

$$|\chi_L\rangle = \frac{1}{\sqrt{L}} \sum_{i=1}^L |\psi_i\rangle|i\rangle \quad (\text{S16})$$

where the data state is the partial trace $\text{tr}_B(\cdot)$ over the L ancilla degrees of freedom $|i\rangle$

$$\rho_L = \text{tr}_B(|\chi_L\rangle\langle\chi_L|) = \sum_{i=1}^L (I_N \otimes \langle i|) |\chi_L\rangle\langle\chi_L| (I_N \otimes |i\rangle) = \frac{1}{L} \sum_{i=1}^L |\psi_i\rangle\langle\psi_i|. \quad (\text{S17})$$

We now define the evolved purified state $U(\boldsymbol{\theta}) \otimes I_B |\chi_L\rangle$ where I_B with $\dim(I_B) = \log_2(L)$ is the identity over the ancilla qubits of the purification degrees of freedom. A straightforward calculation shows that the QFIM \mathcal{F}_{nm} of the purified data state is equivalent to the DQFIM $\mathcal{Q}_{nm}(\rho_L, U(\boldsymbol{\theta}))$ via

$$\begin{aligned}
& \mathcal{F}_{nm}(U(\boldsymbol{\theta}) \otimes I_B |\chi_L\rangle) = \\
& 4\text{Re}(\langle\chi_L| \partial_n U(\boldsymbol{\theta})^\dagger \otimes I_B \partial_m U(\boldsymbol{\theta}) \otimes I_B |\chi_L\rangle - \langle\chi_L| U(\boldsymbol{\theta})^\dagger \otimes I_B \partial_n U(\boldsymbol{\theta}) \otimes I_B |\chi_L\rangle \langle\chi_L| \partial_m U(\boldsymbol{\theta})^\dagger \otimes I_B U(\boldsymbol{\theta}) \otimes I_B |\chi_L\rangle) = \\
& 4\text{Re}(\frac{1}{L} \sum_{ij} \langle\psi_i| \langle i| \partial_n U(\boldsymbol{\theta})^\dagger \otimes I_B \partial_m U(\boldsymbol{\theta}) \otimes I_B |\psi_j\rangle |j\rangle - \\
& \frac{1}{L^2} \sum_{ij} \langle\psi_i| \langle i| U(\boldsymbol{\theta})^\dagger \otimes I_B \partial_n U(\boldsymbol{\theta}) \otimes I_B |\psi_j\rangle |j\rangle \sum_{ij} \langle\psi_i| \langle i| \partial_m U(\boldsymbol{\theta})^\dagger \otimes I_B U(\boldsymbol{\theta}) \otimes I_B |\psi_j\rangle |j\rangle) = \\
& 4\text{Re}(\frac{1}{L} \sum_i \langle\psi_i| \partial_n U(\boldsymbol{\theta})^\dagger \partial_m U(\boldsymbol{\theta}) |\psi_i\rangle - \frac{1}{L^2} \sum_i \langle\psi_i| U(\boldsymbol{\theta})^\dagger \partial_n U(\boldsymbol{\theta}) |\psi_i\rangle \sum_i \langle\psi_i| \partial_m U(\boldsymbol{\theta})^\dagger U(\boldsymbol{\theta}) |\psi_i\rangle) = \\
& 4\text{Re}(\text{tr}(\frac{1}{L} \sum_i |\psi_i\rangle\langle\psi_i| \partial_n U(\boldsymbol{\theta})^\dagger \partial_m U(\boldsymbol{\theta})) - \text{tr}(\frac{1}{L} \sum_i |\psi_i\rangle\langle\psi_i| U(\boldsymbol{\theta})^\dagger \partial_n U(\boldsymbol{\theta})) \text{tr}(\sum_i \frac{1}{L} |\psi_i\rangle\langle\psi_i| \partial_m U(\boldsymbol{\theta})^\dagger U(\boldsymbol{\theta}))) = \\
& 4\text{Re}(\text{tr}(\partial_m U(\boldsymbol{\theta}) \rho_L \partial_n U(\boldsymbol{\theta})^\dagger) - \text{tr}(\partial_n U(\boldsymbol{\theta}) \rho_L U(\boldsymbol{\theta})^\dagger) \text{tr}(U(\boldsymbol{\theta}) \rho_L \partial_m U(\boldsymbol{\theta})^\dagger)) = \mathcal{Q}_{nm}(\rho_L, U(\boldsymbol{\theta})).
\end{aligned}$$

We now propose two measurement scheme for the DQFIM for experiments on quantum computers.

4. Measuring DQFIM on quantum computers using Hadamard test

We now propose an approach to measure the DQFIM using the Hadamard test.

First note that that our ansatz Eq. (S1) consist of G layers with

$$U(\boldsymbol{\theta}) = \prod_{k=1}^G U_k(\boldsymbol{\theta}_k) \text{ with } U^{(k)}(\boldsymbol{\theta}_k) = \prod_{n=1}^K \exp(-i\theta_{kn}H_n) \quad (\text{S18})$$

where $U^{(k)}(\boldsymbol{\theta}_k)$ is the unitary of the k th layer. Here, H_n are K hermitian matrices and $\boldsymbol{\theta}_k = \{\theta_{k1}, \dots, \theta_{kn}\}$ are the parameters of the k th layer. The total parameter vector $\boldsymbol{\theta} = \{\boldsymbol{\theta}_1, \dots, \boldsymbol{\theta}_G\}$ of the ansatz has $M = GK$ parameters.

As we have $\partial_n \exp(-i\theta_n H_n) = -iH_n \exp(-i\theta_n H_n)$, we can write the derivatives as

$$\partial_n U(\boldsymbol{\theta}) = -iU_{n+1 \rightarrow M} H_n U_{1 \rightarrow n}. \quad (\text{S19})$$

Here, we define

$$U_{m \rightarrow n} = U_n U_{n-1} \dots U_{m+1} U_m \quad (\text{S20})$$

as the propagator from layer m to layer n .

We have the DQFIM with

$$\mathcal{Q}_{nm}(\rho_L) = 4\text{Re}(\text{tr}(\partial_n U \rho_L \partial_m U^\dagger) - \text{tr}(\partial_n U \rho_L U^\dagger) \text{tr}(U \rho_L \partial_m U^\dagger)).$$

First, computing $\text{tr}(U \rho_L \partial_m U^\dagger)$ and $\text{tr}(\partial_n U \rho_L U^\dagger)$ is straightforward as they are observables. In particular, using $\rho_L = \frac{1}{L} \sum_{i=1}^L |\psi_i\rangle\langle\psi_i|$ and Eq. (S7) we have

$$\text{tr}(\partial_n U \rho_L U^\dagger) = \frac{1}{L} \sum_{i=1}^L \langle\psi_i|U^\dagger \partial_n U|\psi_i\rangle = \frac{1}{L} \sum_{i=1}^L \langle\psi_i|U^\dagger U_{n+1 \rightarrow M} (-iH_n) U_{1 \rightarrow n} |\psi_i\rangle = \frac{-i}{L} \sum_{i=1}^L \langle\psi_i|U_{1 \rightarrow n}^\dagger H_n U_{1 \rightarrow n} |\psi_i\rangle$$

i.e. one needs to simply evolve each training state with $U_{1 \rightarrow n} |\psi_i\rangle$ and measure the operator H_n . Similarly, one measures $\text{tr}(U \rho_L \partial_m U^\dagger)$.

Next, we measure $\text{Re}(\text{tr}(\partial_n U \rho_L \partial_m U^\dagger))$ which is not an observable, but can be efficiently measured using the Hadamard test [93, 94]. In particular, assuming $n > m$ we have

$$\begin{aligned} \text{Re}(\text{tr}(\partial_n U \rho_L \partial_m U^\dagger)) &= \frac{1}{L} \sum_{i=1}^L \text{Re}(\langle\psi_i|\partial_m U^\dagger \partial_n U|\psi_i\rangle) = \\ &= \frac{1}{L} \sum_{i=1}^L \text{Re}(\langle\psi_i|U_{1 \rightarrow n}^\dagger (iH_m) U_{m+1 \rightarrow M}^\dagger U_{n+1 \rightarrow M} (-iH_n) U_{1 \rightarrow n} |\psi_i\rangle) = \frac{1}{L} \sum_{i=1}^L \text{Re}(\langle\psi_i|U_{1 \rightarrow m}^\dagger H_m U_{m+1 \rightarrow n}^\dagger H_n U_{1 \rightarrow n} |\psi_i\rangle) \end{aligned}$$

Terms of the form $\text{Re}(\langle\psi_i|U_{1 \rightarrow m}^\dagger H_m U_{m+1 \rightarrow n}^\dagger H_n U_{1 \rightarrow n} |\psi_i\rangle)$ can be efficiently measured using the Hadamard test described in [94]. It requires one ancilla qubit, and replacing H_m, H_n with controlled operators, e.g. $H_n = \sigma_1^x$ becomes a CNOT with control on the ancilla and target on the first qubit. So in total, we require a single ancilla and two two-qubit control operations for circuits composed of parameterized single-qubit rotations and arbitrary entangling gates.

5. Measuring DQFIM on quantum computers using shift-rule and purification

Now, we propose to measure the DQFIM using its purification and the shift-rule. This method requires preparing the purification of ρ_L , and then uses the standard shift-rule to efficiently measure the DQFIM.

It has been shown that the QFIM can be efficiently measured. In particular, one can show that the QFIM is the Hessian of the fidelity [85, 91] via

$$\mathcal{F}_{nm} = -\frac{1}{2} \partial_n \partial_m |\langle\chi(\boldsymbol{\theta})|\chi(\boldsymbol{\theta}_0)\rangle|_{\boldsymbol{\theta}_0=\boldsymbol{\theta}} \quad (\text{S21})$$

and one can use the shift-rule to efficiently measure the QFIM [85] given ansatz Eq. (S1). As we have shown above the DQFIM for data state $\rho_L = L^{-1} \sum_i |\psi_i\rangle\langle\psi_i|$ and unitary $U(\boldsymbol{\theta})$ is equivalent to the QFIM for the purified state

$$|\chi(\boldsymbol{\theta})\rangle = \frac{1}{\sqrt{L}} \sum_{i=1}^L U(\boldsymbol{\theta}) \otimes I_B |\psi_i\rangle|i\rangle \quad (\text{S22})$$

where we have

$$\mathcal{Q}_{nm}(\rho_L, U(\boldsymbol{\theta})) = \mathcal{F}_{nm}(|\chi(\boldsymbol{\theta})\rangle). \quad (\text{S23})$$

Now that we relate the DQFIM to the QFIM of the purification, we can harness known results of efficiently measuring the QFIM.

Using the shift-rule for the QFIM from Ref. [85], we get

$$\begin{aligned} \mathcal{Q}_{nm}(\boldsymbol{\theta}) = & -\frac{1}{8} [|\langle \chi(\boldsymbol{\theta}) | \chi(\boldsymbol{\theta} + (\mathbf{e}_n + \mathbf{e}_m)\pi/2) \rangle|^2 - |\langle \chi(\boldsymbol{\theta}) | \chi(\boldsymbol{\theta} + (\mathbf{e}_n - \mathbf{e}_m)\pi/2) \rangle|^2 - \\ & |\langle \chi(\boldsymbol{\theta}) | \chi(\boldsymbol{\theta} + (-\mathbf{e}_n + \mathbf{e}_m)\pi/2) \rangle|^2 + |\langle \chi(\boldsymbol{\theta}) | \chi(\boldsymbol{\theta} - (\mathbf{e}_n + \mathbf{e}_m)\pi/2) \rangle|^2], \end{aligned} \quad (\text{S24})$$

where \mathbf{e}_n is the basis vector for n -th index of parameter vector $\boldsymbol{\theta}$. After preparing the purification, one can then efficiently measure the overlaps $|\langle \chi(\boldsymbol{\theta}) | \chi(\boldsymbol{\theta} + (\mathbf{e}_n + \mathbf{e}_m)\pi/2) \rangle|^2$ via the inversion test or SWAP test (see Appendix G of Ref. [49] for a review).

Supplemental Materials B: Degrees of freedom of isometries

Now, we calculate the degrees of freedom when learning a training set of L states with a d -dimensional unitary

$$U = \sum_{n,k=1}^d u_{nk} |n\rangle \langle k| \quad (\text{S1})$$

with $u_{nk} = a_{nk} + ib_{nk}$, where a_{nk}, b_{nk} are real parameters. First, note that U can be described using $2d^2$ real parameters, however due to $U^\dagger U = I$ and global phase, only $d^2 - 1$ real parameters are independent. We now compute the maximal number of degrees of freedom when U is projected onto a training set of L states. For any set S_L of training states, the rank of ρ_L and equivalently its projector onto the subspace of non-zero eigenvalues Π_L is upper bounded by $\text{rank}(\rho_L) = \text{rank}(\Pi_L) \leq L$.

We apply U Eq. (S1) on a training set $\{|\ell\rangle\}_{\ell=1}^L$ of L states, where $|\ell\rangle$ are computational basis states. For a single training state $L = 1$, we have $U|1\rangle = \sum_{n=1}^d u_{n1}|n\rangle$. Via training, we can only learn the column vector $u_1 = (u_{11}, u_{21}, \dots, u_{d1})$, which has $2d$ real parameters and $2d - 2$ independent parameters due to constraints of global phase and norm $\sum_{n=1}^d |u_{n1}|^2 = 1$. However, all other column vectors besides u_1 cannot be learned. With the DQFIM we find $R_1 = 2d - 2$, i.e. R_1 indeed counts the number of degrees of freedom that can be learned. Next, we consider $L = 2$. Here, we additionally have the state $U|2\rangle = \sum_{n=1}^d u_{n2}|n\rangle$ and we can also learn the vector $u_2 = (u_{12}, u_{22}, \dots, u_{d2})$ with $2d$ real parameters. However, due to unitarity, u_2 must be orthogonal to u_1 , which removes two degrees of freedom. Additionally, we have to subtract one parameter for the norm condition. The global phase has already been incorporated in u_1 , thus u_2 holds $2d - 3$ degrees of freedom, with the $d \times 2$ -dimensional isometry (u_1, u_2) combined having $R_2 = 4d - 5$. For any L , each additional training state adds a column u_L , which has additional $2d - 2L + 1$ degrees of freedom due to $L - 1$ orthogonality conditions [73]. For L states, we have the isometry $U_L = (u_1, \dots, u_L)$, which can be described using

$$R_L = (2d - 2)L - (L - 1)^2 = 2dL - L^2 - 1 \quad (\text{S2})$$

real independent parameters and for $L \geq 1$. The maximum is reached for $L_c = d$ with $R_d = d^2 - 1$ and $U\Pi_d = U$ with $\Pi_d = I$, where we can completely learn U . For further increase in L we find that R_L stays constant. As our choice of U is a generic representation of a unitary and our chosen training set has maximal rank $\text{rank}(\Pi_L) = L$, our calculation gives us the upper bound for R_L . Note that by choosing a more constrained ansatz unitary and training sets R_L can be smaller.

For an arbitrary unitary, the gain in effective dimension by increasing dataset size $L \rightarrow L + 1$ is given by $\Delta R_L = R_{L+1} - R_L = \max(2d - 2L - 1, 0)$ for $L \geq 1$, and $\Delta R_0 = 2d - 2$ for $L = 0$. Thus, the gain decreases with L , i.e. with increasing L each additional state reveals less degrees of information of U .

Supplemental Materials C: Lie-algebra bound on the rank of DQFIM

Recall that our ansatz Eq. (S1) consist of G layers with

$$U(\boldsymbol{\theta}) = \prod_{k=1}^G U_k(\boldsymbol{\theta}_k) \text{ with } U^{(k)}(\boldsymbol{\theta}_k) = \prod_{n=1}^K \exp(-i\theta_{kn}H_n) \quad (\text{S1})$$

where $U^{(k)}(\boldsymbol{\theta}_k)$ is the unitary of the k th layer. Here, H_n are K hermitian matrices and $\boldsymbol{\theta}_k = \{\theta_{k1}, \dots, \theta_{kn}\}$ are the parameters of the k th layer. The total parameter vector $\boldsymbol{\theta} = \{\boldsymbol{\theta}_1, \dots, \boldsymbol{\theta}_G\}$ of the ansatz has $M = GK$ parameters.

To simplify the notation, we treat each parameter entry as its own layer and relabel each generators H_k such that we can write the ansatz as

$$U(\boldsymbol{\theta}) = \prod_{k=1}^M \exp(-i\theta_k H_k). \quad (\text{S2})$$

First, we define the generators of the ansatz U [59, 95]:

Definition 5 (Set of generators \mathcal{T}). *Consider ansatz Eq. (S2). The set of generators $\mathcal{T} = \{H_k\}_{k=1}^K$ (with size $|\mathcal{T}| = K$) are defined as the set of Hermitian operators that generate the unitaries of each layer of $U(\boldsymbol{\theta})$.*

Further the dynamical Lie Algebra \mathfrak{g} is given by:

Definition 6 (Dynamical Lie Algebra (DLA)). *Consider the generators \mathcal{T} according to Def. 5. The DLA \mathfrak{g} is generated by repeated nested commutators of the operators in \mathcal{T}*

$$\mathfrak{g} = \text{span} \langle iH_1, \dots, iH_K \rangle_{Lie}, \quad (\text{S3})$$

where $\langle S \rangle_{Lie}$ is the Lie closure, which is the set obtained by repeatedly taking the commutator of the elements in S .

Next, we show that the DLA bounds the rank of the DQFIM. First, lets recall the entries of the matrix of the DQFIM

$$\mathcal{Q}_{nm}(S_L, U(\boldsymbol{\theta})) = 4\text{Re}(\text{tr}(\partial_n U \rho_L \partial_m U^\dagger) - \text{tr}(\partial_n U \rho_L U^\dagger) \text{tr}(U \rho_L \partial_m U^\dagger)). \quad (\text{S4})$$

where we shorten $U = U(\boldsymbol{\theta})$ and $\partial_n U$ the derivative in respect to the n th element of parameter vector $\boldsymbol{\theta}$.

We now restate Theorem 1 of the main text for convenience.

Theorem 2. *The maximal rank R_L of the DQFIM is upper bounded by the dimension of the dynamical Lie algebra (DLA) $\dim(\mathfrak{g})$*

$$R_L \leq \dim(\mathfrak{g}), \quad (\text{S5})$$

where $\mathfrak{g} = \text{span} \langle iH_1, \dots, iH_K \rangle_{Lie}$ is generated by the repeated nested commutators of the generators H_k of the unitary $U(\boldsymbol{\theta})$.

The proof follows in analogy to the bound of the QFIM (i.e. R_1) of Ref. [59].

First, we note that $R_L \leq R_\infty$ as L simply increases the dimension spanned by the dataset ρ_L . Now, we assume S_L spans the complete relevant Hilbertspace with $\rho_L = I/d$ and thus we can simplify to the unitary QFIM

$$\mathcal{Q}_{nm} = 4\text{Re}(d^{-1} \text{tr}(\partial_n U \partial_m U^\dagger) - d^{-2} \text{tr}(\partial_n U U^\dagger) \text{tr}(U \partial_m U^\dagger)). \quad (\text{S6})$$

As we have $\partial_n \exp(-i\theta_n H_n) = -iH_n \exp(-i\theta_n H_n)$, we can write the derivatives as

$$\partial_n U(\boldsymbol{\theta}) = -iU_{n+1 \rightarrow M} H_n U_{1 \rightarrow n}. \quad (\text{S7})$$

Here, we define

$$U_{m \rightarrow n} = U_n U_{n-1} \dots U_{m+1} U_m \quad (\text{S8})$$

as the propagator from layer m to layer n and

$$\tilde{H}_k = U_{1 \rightarrow k}^\dagger H_k U_{1 \rightarrow k}. \quad (\text{S9})$$

Using above expressions, we find for the first term of the DQFIM Eq. (S6)

$$\text{Re}(\text{tr}(\partial_n U \partial_m U^\dagger)) = \text{Re}(i(-i)\text{tr}(U_{n+1 \rightarrow M} H_n U_{1 \rightarrow n} U_{1 \rightarrow m}^\dagger H_m U_{m+1 \rightarrow M}^\dagger)) = \text{Re}(\text{tr}(\tilde{H}_n \tilde{H}_m)).$$

Similarly, we find for the second term of Eq. (S6)

$$\text{Re}(\text{tr}(\partial_n U U^\dagger) \text{tr}(U \partial_m U^\dagger)) = \text{Re}(i(-i)\text{tr}(U_{n+1 \rightarrow M} H_n U_{1 \rightarrow n} U_{1 \rightarrow M}^\dagger) \text{tr}(U_{1 \rightarrow M} U_{1 \rightarrow m}^\dagger H_m U_{m+1 \rightarrow M}^\dagger)) = \text{Re}(\text{tr}(\tilde{H}_n) \text{tr}(\tilde{H}_m)).$$

We combine these results to get the DQFIM as

$$\mathcal{Q}_{mn}^I = \text{Re}(d^{-1} \text{tr}(\tilde{H}_n \tilde{H}_m) - d^{-2} \text{tr}(\tilde{H}_n) \text{tr}(\tilde{H}_m)) \quad (\text{S10})$$

Note that H_k are elements of the DLA \mathfrak{g} . As the unitaries U_n of the ansatz are also elements of the dynamical Lie group generated by \mathfrak{g} , a product of H_k with any U_n will yield another element of the dynamical Lie group. Thus, we can always expand \tilde{H}_k using the DLA as a basis with $\dim(\mathfrak{g})$ elements:

$$\tilde{H}_k = \sum_{m=1}^{\dim(\mathfrak{g})} a_m^{(k)} \chi_m, \quad (\text{S11})$$

where $a_m^{(k)}$ are real coefficients and $\{\chi_m\}_{m=1}^{\dim(\mathfrak{g})}$ are a basis of the DLA \mathfrak{g} . Thus, the matrix of the DQFIM \mathcal{Q} can be expressed in a basis with $\dim(\mathfrak{g})$ elements. Thus, the rank of \mathcal{Q} is upper bounded by the dimension of the DLA \mathfrak{g}

$$R_L \leq \text{rank}(\mathcal{Q}^I) \leq \dim(\mathfrak{g}). \quad (\text{S12})$$

Supplemental Materials D: Ansatz unitaries

The ansatz unitaries used in the main text are shown in Fig. S1. We assume that the considered unitaries have a periodic structure of G layers with

$$U(\theta) = \prod_{k=1}^G U_k(\theta_k), \quad U^{(k)}(\theta_k) = \prod_{n=1}^K \exp(-i\theta_{kn} H_n) \quad (\text{S1})$$

where $U^{(k)}(\theta_k)$ is the unitary of the k th layer. Here, H_n are K hermitian matrices and $\theta_k = \{\theta_{k1}, \dots, \theta_{kn}\}$ are the parameters of the k th layer. The total parameter vector $\theta = \{\theta_1, \dots, \theta_G\}$ of the ansatz has $M = GK$ parameters.

In Fig.S1a, we show a hardware efficient ansatz U_{HE} , which produces highly random circuits which span the full Hilbertspace nearly uniformly and are known to be hard to simulate classically. Overparameterization requires for this circuit exponentially many parameters.

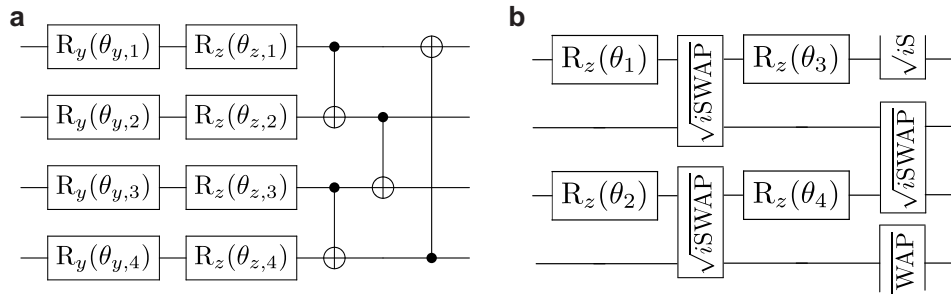


FIG. S1. Ansatz unitaries for the main text. The circuits are repeated for G layers. **a)** Hardware-efficient ansatz U_{HE} consisting of parameterized y, z rotations and CNOT gates. Has no symmetries and can realize arbitrary N -qubit unitaries for sufficient depth. **b)** U_{XY} circuit inspired by XY-model Eq. (S2). Composed of single qubit z rotations and nearest-neighbor \sqrt{i} SWAP gates, arranged with periodic boundary condition. Commutes with particle number operator P .

In Fig.S1b, we show an ansatz U_{XY} that overparameterizes in polynomial depth. This ansatz is inspired from the integrable XY Hamiltonian with random field h_k

$$H_{XY} = \sum_{k=1}^N h_k \sigma_k^z + \sum_{k=1}^N (\sigma_k^x \sigma_{k+1}^x + \sigma_k^y \sigma_{k+1}^y) \quad (\text{S2})$$

H_{XY} commutes with the particle number operator $P = \sum_{k=1}^N \frac{1}{2}(1 - \sigma_k^z)$ where σ_k^z is the Pauli z operator acting on qubit k . In particular, we have $[H_{XY}, P]$. Its time evolution $U = \exp(-iH_{XY}t)$ also conserves the symmetry, i.e. $[U, P] = 0$.

The ansatz U_{XY} shown in S1b can represent the time evolution of the Hamiltonian. U_{XY} consists of parameterized z -rotations and nearest-neighbor \sqrt{i} SWAP $= \exp(i\pi/8(\sigma_k^x \sigma_{k+1}^x + \sigma_k^y \sigma_{k+1}^y))$ gates. The ansatz conserves particle number symmetry as well, i.e. $[U_{XY}, P] = 0$. One can think of this model similar to a Trotterized version of the time evolution $U = \exp(-iH_{XY}t)$. The generators of U_{XY} are the Pauli operators of H_{XY} . Thus, the time-evolution operator U_{XY} spans the same dynamical Lie algebra as the time evolution generated by H_{XY} and can represent any time evolution of H_{XY} [75]. The dimension of the dynamical Lie-algebra spanned by U_{XY} scales polynomially with qubit number N and thus can be overparameterized with polynomially many parameters M [59]. For random product states W_{prod} as training set, we find via numerical extrapolation $R_1 = 2N^2 - 3N + 2$ and $R_\infty = 2N^2 - 1$. As another training set, we choose $W_{p=1}$ with $P = 1$ particles, which consists of arbitrary superpositions of permutations of the basis states $|10\dots 0\rangle$. We have $P|\psi_\ell\rangle = |\psi_\ell\rangle$ for any state $|\psi_\ell\rangle \in W_{p=1}$. These states live in an effective N -dimensional subspace, yielding $R_1 = 2N - 2$ and $R_\infty = N^2 - 1$.

Supplemental Materials E: Additional results on XY circuit learning

We now show additional numerical results on training with the U_{XY} ansatz which conserves particle number.

In Fig. S2, we study overparameterization and generalization as function of M . We study test and training error for the U_{XY} ansatz for training with product state ensemble W_{prod} . Using the analytic rank of DQFIM of the main text, we find $L_c \approx 2$. For sufficient M , we have $C_{\text{train}} \approx 0$ for $L = 1$ and $L = 2$ training data. Generalization with $C_{\text{test}} \approx 0$ requires $L \geq 2$ when testing in-distribution W_{prod} or out-of-distribution $W_{p=1}$, matching the result predicted using the DQFIM.

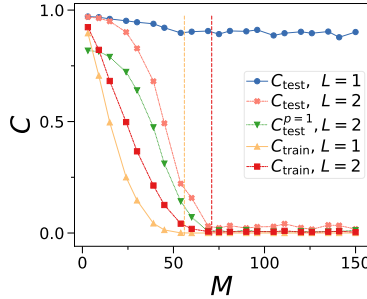


FIG. S2. Unitary learning with U_{XY} ansatz. We show C_{test} and C_{train} against M with U_{XY} ansatz for $N = 6$ qubits, where we train with $L = 1$ and $L = 2$ product states W_{prod} . We use W_{prod} as test states, except for green dotted curve $C_{\text{test}}^{p=1}$ where we show out-of-distribution generalization with symmetric test states $W_{p=1}$. The dashed vertical lines indicate R_1 (yellow) and R_2 (red).

Now, we use training data which respects particle number $P = \sum_{k=1}^N \frac{1}{2}(1 - \sigma_k^z)$, i.e. the training states are sampled from $W_{p=1}$ which are states with Hamming weight 1. Using the rank of the DQFIM, we compute $L_c \approx 2R_\infty/R_1 \approx N$.

In Fig. S3a we study C_{test} against L, M for U_{XY} when training with particle-conserved ensemble $W_{p=1}$. Generalization improves with M and L , where the lower bound $C_{\text{test}} \sim 1 - (L/L_c)^2$ [6] is saturated for $M \geq M_c$. In Fig. S3b, we study generalization in the overparameterized regime. We find $C_{\text{test}} \sim 1 - (L/L_c)^2$ independent of N , which matches the theoretical result of Ref. [6]. In Fig. S3c, we find that for overparameterized models $E \sim N^2$ with a clear peak at $L \approx L_c$. In Fig. S3d we study the steps E needed to converge against M for different N for overcomplete data $L \gg L_c$. We observe $E \sim N^2$. At M_c the steps needed to converge sharply decreases, indicating the transition to an optimization landscape where the global minimum can be reached easily.

Fig. S4, we show C_{train} , C_{test} and number of iterations E against L and M for symmetric data $W_{p=1}$. We find training and test error matches closely the transitions derived from R_L which are shown as black dashed lines.

Next, in Fig.S5a-c we study C_{train} and C_{test} for the U_{XY} ansatz. Here, we train using random product states W_{prod} which do not respect particle number symmetry. Here, we generalize already for $L \geq 2$.

Next, in Fig.S5d we study out-of-distribution generalization with the U_{XY} ansatz. Here, the training states are

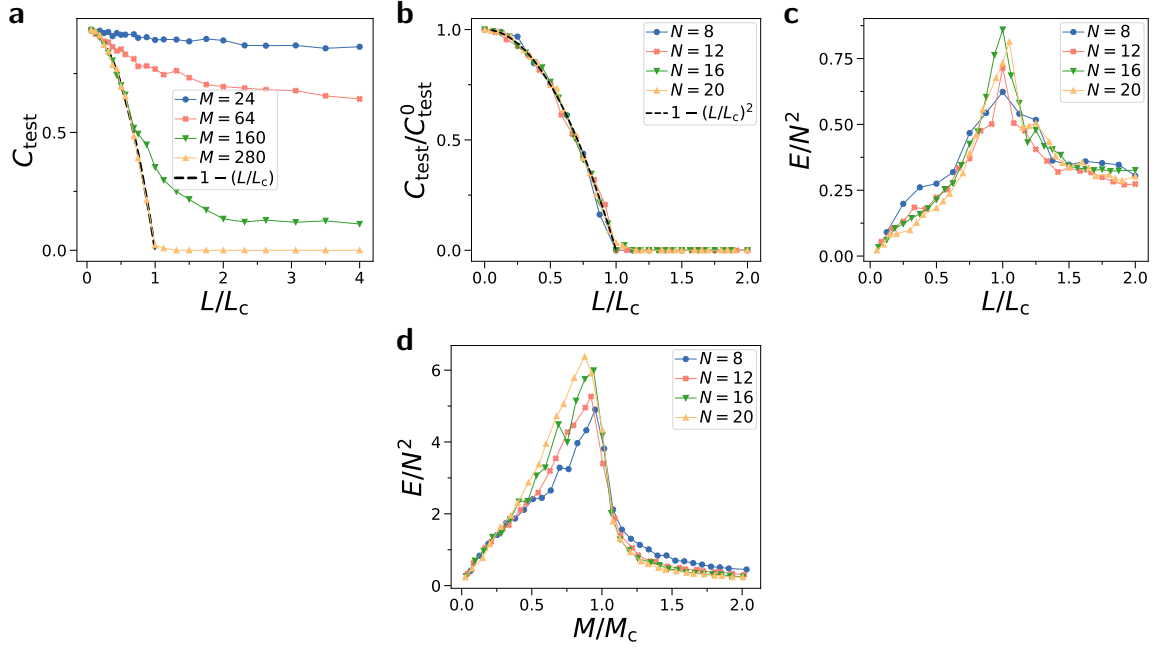


FIG. S3. Unitary learning of particle number conserving ansatz $U_{XY}(\theta)$ with symmetric states $|\psi_\ell\rangle \in W_{p=1}$. **a)** C_{test} against L for different M with $N = 16$, $L_c = N$. Black dashed line is $C_{\text{test}} \sim 1 - (L/L_c)^2$. **b)** Test error C_{test} relative to error without training C_{test}^0 for varying training set size L and $M \gg M_c$ where we use symmetric data $|\psi_\ell\rangle \in W_{p=1}$. We find $C_{\text{test}}/C_{\text{test}}^0 = 1 - (L/L_c)^2$, where $L_c = N$ and we average over 10 random instances. **c)** Training steps E needed to converge to $C_{\text{train}} < 10^{-4}$ against L for $M \gg M_c$. **d)** Training steps E required to find $C_{\text{test}} < 10^{-3}$.

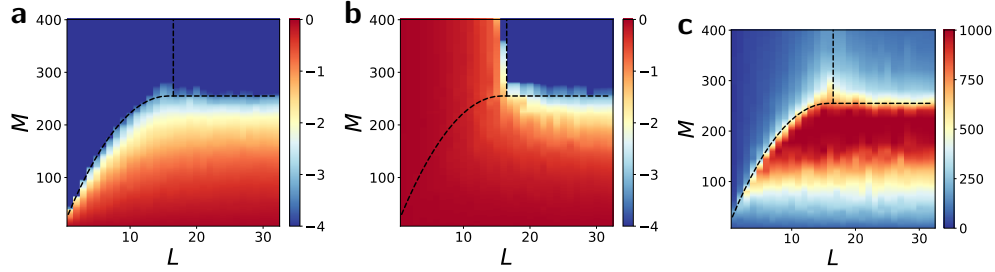


FIG. S4. Median error for training U_{XY} for symmetric data $W_{p=1}$ for $N = 16$ qubits. **a)** C_{train} against M and L . Color shows logarithm $\log_{10}(C_{\text{train}})$. **b)** C_{test} against M and L . **c)** Number of training steps E until reaching $C_{\text{train}} < 10^{-3}$.

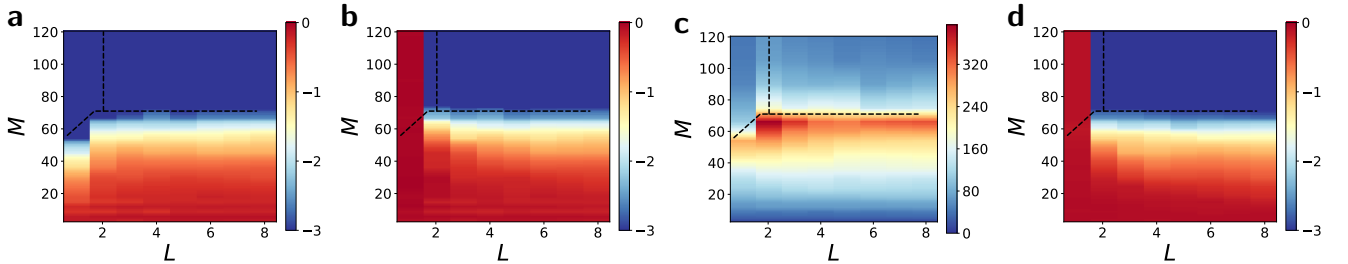


FIG. S5. Median error for training U_{XY} ansatz for random product state data sampled from W_{prod} and $N = 6$ qubits. **a)** C_{train} against M and L . Color shows logarithm $\log_{10}(C_{\text{train}})$. **b)** C_{test} against M and L tested against W_{prod} . **c)** Number of training steps E until reaching $C_{\text{train}} < 10^{-3}$. **d)** Out-of-distribution generalization C_{test} against M and L , where we trained with W_{prod} , but tested with $W_{p=1}$.

drawn from set of product states W_{prod} which break particle number symmetry $P = \sum_{k=1}^N \frac{1}{2}(1 - \sigma_k^z)$, i.e. $P|\psi\rangle$. However, the test data is drawn from a different distribution $W_{p=1}$ (states with Hamming weight 1) which conserve particle number symmetry P . We find that although we train with a different distribution that we use for testing, we achieve the same test error as when training directly with W_{prod} . In particular, we generalize for $L \geq 2$.

In contrast, for in-distribution generalization where one both trains and test with states from $W_{p=1}$ (which respect particle number symmetry), we achieve generalization only for $L \geq N$, where N is the number of qubits. Refer to Fig. S3a of C_{test} against L .

Supplemental Materials F: Generalization with further circuit models

We now study further circuit models which were used to study generalization in other publications. In Fig.S6 we show three ansatz unitaries which we then proceed to study.

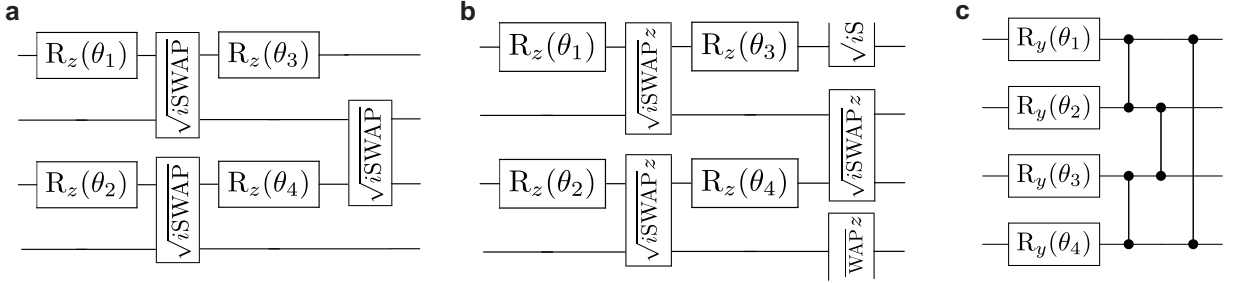


FIG. S6. Ansatz unitaries for the supplemental materials. The circuits are repeated for G layers. **a)** U_{XY}^{open} circuit with open boundary condition, i.e. the $\sqrt{i}\text{SWAP}$ do not cross from the first to the last qubit in contrast to U_{XY} . Commutes with particle number operator P and for sufficient depth can realize any time evolution generated by $\exp(-iH_{XY}^{\text{open}}t)$. **b)** U_{XXZ} circuit related to evolution of Heisenberg model H_{XXZ} . Composed of parameterized single qubit z rotations and the $\sqrt{i}\text{SWAP}_z$ gate defined in the text. **c)** Real-valued ansatz U_{Y-CZ} consisting of y -rotations and control- Z gates in a nearest-neighbor chain configuration.

In Fig.S6a we show the U_{XY}^{open} circuit, which is the same as the U_{XY} circuit but with open boundary conditions, i.e. the $\sqrt{i}\text{SWAP}$ gates that interact between the first and last qubit are removed. This ansatz conserves particle number P .

In Fig.S6b we show the U_{XXZ} ansatz, which is composed of parameterized z rotations and the $\sqrt{i}\text{SWAP}_z = \sqrt{\text{CZ}}\sqrt{i}\text{SWAP}$ gate, where $\sqrt{\text{CZ}} = \text{diag}(1, 1, 1, i)$ is the square-root of the control- Z gate. This ansatz conserves particle number P .

In Fig.S6c we show the U_{Y-CZ} ansatz [49], consisting of parameterized y -rotations and control- Z gate $\text{diag}(1, 1, 1, -1)$. Due to its connection to Cluster-state generation, it overparameterizes with a polynomial number of parameters with $R_L \propto N^2$.

Here, we study the number of training states needed for generalization for the above describe ansatze for the unitary learning task. First, in Fig.S7a we study the U_{XY}^{open} ansatz shown in Fig.S6a. This ansatz describes the evolution of the $H_{XY}^{\text{open}} = \sum_{k=1}^N h_k \sigma_k^z + \sum_{k=1}^{N-1} (\sigma_k^x \sigma_{k+1}^x + \sigma_k^y \sigma_{k+1}^y)$ Hamiltonian with open boundary conditions. The difference to H_{XY} is the absence of interaction between first and last qubit. We find generalization for $L = 1$ training states and $M \geq M_c$ when using random product states as training data. A similar ansatz was studied numerically in Ref. [10]. It was shown numerically that only 1 training state was needed for generalization, and $O(N^2)$ gates for successful training. Here, we explain this result with the DQFIM. In particular, our ansatz has the maximal rank of the DQFIM with $R_L = R_1 = R_\infty = N^2$ for all N . This implies that $L_c = 1$ training state is sufficient to get an overcomplete model and achieve generalization.

Next, we study the U_{XXZ} ansatz shown in Fig.S6b. This model can describes the evolution of the $H_{XXZ} = \sum_{k=1}^N h_k \sigma_k^z + \sum_{k=1}^N (\sigma_k^x \sigma_{k+1}^x + \sigma_k^y \sigma_{k+1}^y + \Delta \sigma_k^z \sigma_{k+1}^z)$ Hamiltonian. A similar ansatz was studied in Ref. [10]. It was numerically shown that 5 training states are needed for generalization for $N = 4$. In Fig.S7b, we show the test error of the U_{XXZ} ansatz against L in the overparameterized regime and indeed find the test error vanishes for $L \geq 5$. Using the DQFIM, we find $R_1 = 24$ and $R_\infty = R_{L_c} = 51$ with $L_c = 5$, matching the numerical results. Thus, the DQFIM accurately predicts the needed training states. Note that the approximation $L_c \approx 2R_\infty/R_1 = 4.25$ gives a good estimation of the number of needed training states as well.

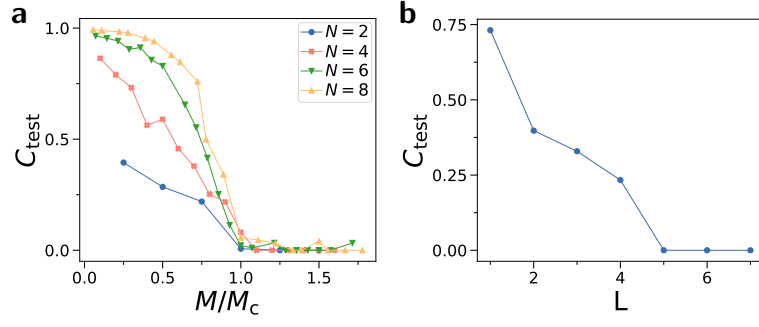


FIG. S7. **a)** Test error C_{test} for U_{XY}^{open} ansatz and for $L = 1$ product training states against circuit parameters M . C_{test} is averaged over 20 random instances. M_c is determined with the DQFIM. **b)** C_{test} for U_{XZZ} ansatz for product training states against L for $N = 4$ and $M = 100$.

We show numerical results on training with the U_{Y-CZ} ansatz (see Fig. S6c for definition) in Fig. S8. This model requires $L = 2$ states to generalize as we have $R_L \sim N^2$. We find training and test error matches closely the transitions derived from R_L shown as black dashed lines.

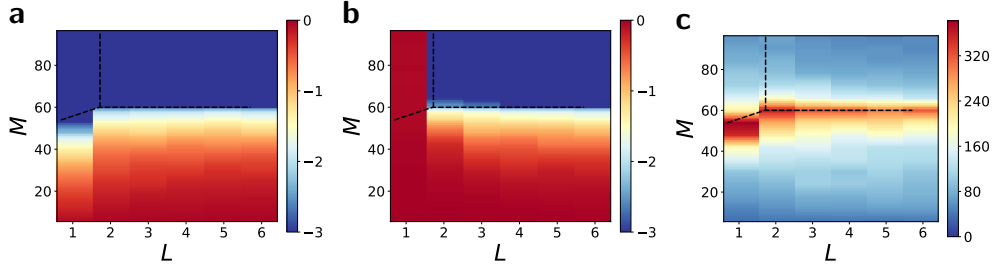


FIG. S8. Median error for training U_{Y-CZ} with product state W_{prod} as training data and $N = 6$ qubits averaged over 10 instances. **a)** C_{train} against M and L . Color shows logarithm $\log_{10}(C_{\text{train}})$. **b)** C_{test} against M and L . **c)** Number of training steps E until reaching $C_{\text{train}} < 10^{-3}$.

Supplemental Materials G: DQFIM for overparameterization and generalization for quantum control

The idea of quantum control is to evolve a quantum system by changing the Hamiltonian parameter in time such that it reaches a desired target state. In particular, we have a time-dependent Hamiltonian [96]

$$H(x(t)) = H_{\text{fix}} + \sum_{k=1}^K x_k(t) H_k \quad (\text{S1})$$

with fixed term H_{fix} and K time-dependent driving terms H_k with strength $x_k(t)$.

Commonly, one discretizes the control terms $x_k(t)$ in time. For example, this is the standard approach for gradient ascent pulse engineering algorithm (GRAPE) [97]. In particular, we discretize time t into B time-steps δt where for the b th timestep $x_k(b\delta t)$ to $x_k((b+1)\delta t)$ the control parameter is kept constant. This gives us $M = KB$ driving parameters $\mathbf{x} = \{x_k(b\delta t)\}_{k=1, b=1}^{K, B}$ with time evolution over total time $T = \delta t B$

$$U(\mathbf{x}) = \prod_{b=1}^B \exp(-iH(x(\delta tb))\delta t). \quad (\text{S2})$$

Now, the goal is to find the driving terms x such that they realize target states $\{|\psi_\ell\rangle\}_{\ell=1}^L$ starting from initial state $\{|\phi_\ell\rangle\}_{\ell=1}^L$ where we demand $|\psi_\ell\rangle = U(\mathbf{x})|\phi_\ell\rangle$ for all $\ell = 1, \dots, L$. Common choices for $|\phi_\ell\rangle$ are the basis states $|\ell\rangle$.

The best control parameters \mathbf{x} are found by optimizing them in respect to the fidelity

$$C_{\text{train}}(\mathbf{x}) = 1 - \frac{1}{L} \sum_{\ell=1}^L |\langle \psi_\ell | U(\mathbf{x}) | \phi_\ell \rangle|^2 = 1 - \frac{1}{L} \sum_{\ell=1}^L \langle \phi_\ell | U(\mathbf{x})^\dagger O_\ell U(\mathbf{x}) | \phi_\ell \rangle. \quad (\text{S3})$$

where we define the label operator $O_\ell = |\psi_\ell\rangle\langle\psi_\ell|$ which describes the target state. Thus, the quantum control problem can be mapped onto the unitary learning problem. Similarly, we can also define a test error when the initial states are drawn from some distribution W .

Assuming that the evolution is controllable, i.e. there is a set \mathbf{x} of control parameters that can reach the target state, can one find this set of parameters via an optimization program minimizing $C_{\text{train}}(\mathbf{x})$? It is known that overparameterized problems where one has a large number of controls K and many timesteps B are easily able to find a good solution, while training of underparameterized control models tends to get stuck in local minimas and it is hard to find good solutions [67, 68]. However, how to choose $B = M/K$ to achieve overparameterization for a given model and initial state? Obviously, if B is chosen to small, then it is hard to find a good control protocol, while choosing B too large will yield a control protocol that is more complex than necessary. The rank of the DQFIM tell us at what B the model overparameterizes, which is the best choice of discretization.

We now demonstrate two control problems and show that the maximal rank of the DQFIM allows us to determine the overparameterization transition as function of M and L .

First, we study an Ising Hamiltonian with additional longitudinal field that is known to be non-integrable with the choice

$$H_{\text{fix}} = \sum_{n=1}^N \sigma_n^x \sigma_{n+1}^x + g \sigma_n^x \quad (\text{S4})$$

and the tunable transversal field $H_k = x_k(t) \sigma_k^z$ with $k = 1, \dots, N = K$. We show the result in Fig. S9. We show the training error in Fig. S9a. We find that the training error vanishes beyond a certain $M = B/K$, which is given by the maximal rank of the DQFIM which is shown as dashed line. This is the transition to overparameterization, which also depends on the number of initial states L for the control problem. In Fig. S9b we show the test error against arbitrarily chosen initial states. The vertical dashed line shows the critical number of initial states $L = 2R_\infty/R_1$, which we find matches the transition in the text error accurately. In Fig. S9c we show the number of iterations until the training converges. We find that around $M \sim M_c$, the number of iterations needed becomes much larger.

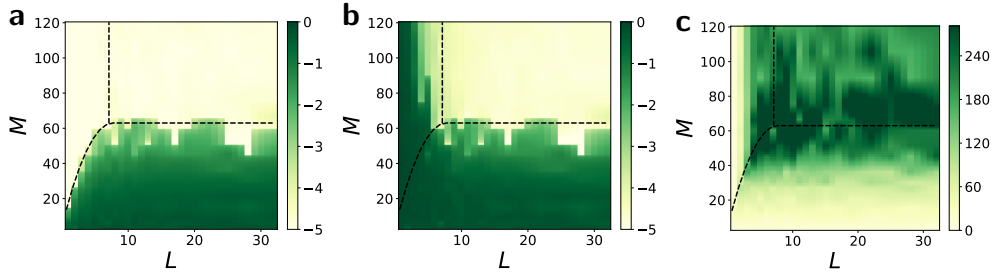


FIG. S9. Fidelity of optimized control protocol \mathbf{x} for non-integrable Ising Hamiltonian Eq. (S4). **a**) Median of trained cost function $\log(C_{\text{train}})$ against number of control parameters M and number of training states L . Black dashed line is maximal rank of DQFIM R_L . **b**) Median of test cost $\log(C_{\text{test}})$. **c**) Number of training steps E until reaching $C_{\text{train}} < 10^{-4}$. We have $N = 3$ qubits, $g = 0.3$, total time $T = 6$ and initial states are random product states and target states are chosen randomly from the feasible control space.

We also study the Heisenberg XXZ Hamiltonian, which is non-integrable but has symmetries which restrict the dynamics to a subspace of the full Hilbertspace [10]. It is given by

$$H_{\text{fix}} = \sum_{n=1}^N \sigma_n^x \sigma_{n+1}^x + \sigma_n^y \sigma_{n+1}^y + g \sigma_n^z \sigma_{n+1}^z \quad (\text{S5})$$

and tunable field $H_k = x_k(t) \sigma_k^z$.

We show the result for the Heisenberg Hamiltonian in Fig. S10. We show the training error after training against L and number of control parameters M in Fig. S10a. The black dashed line is the maximal rank of the DQFIM, which

matches when the training error vanished due to overparameterization. Note that while the Heisenberg model is non-integrable, due its symmetries we require less parameters M to overparameterize than for a generic Hamiltonian (e.g. for $N = 4$ one has overparameterization for $M \geq R_5 = 134$ for $L = 5$, while for Heisenberg model we find overparameterization at much lower M). We show the test error in Fig. S10b, where we find that the test error vanishes for $L \geq 5$, which matches the vertical dashed line which shows the critical $L_{\text{crit}} = 2R_\infty/R_1$. In Fig. S10c, we show the number of iterations until the training converges. We find that close to critical M_c and L_c more iterations are needed to successfully train.

In conclusion, we find that the rank of the DQFIM precisely tells how to discretize control parameters to overparameterize quantum control problems.

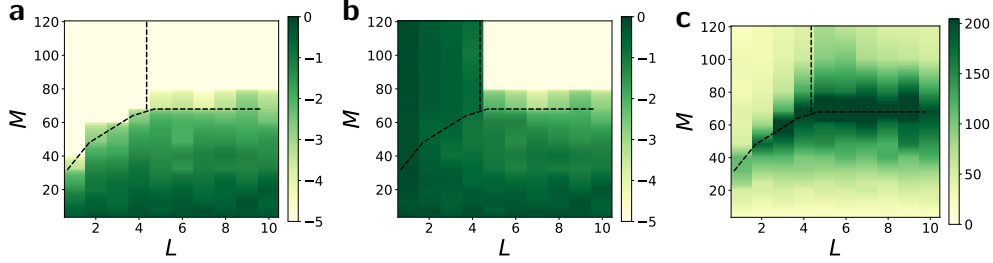


FIG. S10. Fidelity of optimized control protocol \boldsymbol{x} for Heisenberg Hamiltonian Eq. (S5). **a**) Median of trained cost function $\log(C_{\text{train}})$ against control parameters M and number of training states L . Black dashed line is M_c from maximizing rank of DQFIM R_L . **b**) Median of test cost $\log(C_{\text{test}})$. **c**) Number of training steps E until reaching $C_{\text{train}} < 10^{-4}$. We have $N = 4$ qubits, $g = 0.3$, total time $T = 12$ and initial states are random product states and target states are chosen randomly from the feasible control space.

Supplemental Materials H: Overparameterization for generative models

In generative modeling, the goal is to produce samples $x \sim p(x)$ from a probability distribution $p(x)$. In quantum generative learning, called quantum circuit born machines, x is sampled from a quantum state $|\psi(\boldsymbol{\theta})\rangle$ with $p(x) \approx |\langle x|\psi(\boldsymbol{\theta})\rangle|^2$ [32]. The state $|\psi(\boldsymbol{\theta})\rangle$ is trained from samples of the distribution $\{x_\ell\}_{\ell=1}^L$. Various methods to write down cost functions are known which are reviewed in Ref. [63].

Here, we highlight what is called fidelity training, an explicit learning method which can evade barren plateaus for shallow circuits [63]. In this method, the cost function is written as

$$C_{\text{train}}(\boldsymbol{\theta}) = \langle \psi | U^\dagger(\boldsymbol{\theta}) | \Phi \rangle \langle \Phi | U(\boldsymbol{\theta}) | \psi \rangle \quad (\text{S1})$$

with state $|\Phi\rangle = \sum_{\ell=1}^L \sqrt{q(x_\ell)} |x_\ell\rangle$ encoding the training set where $|x_\ell\rangle$ is the basis state corresponding to x_ℓ and $q(x_\ell)$ is the multiplicity of each outcome x_ℓ . Note that this scheme corresponds to learning a unitary with a single $L = 1$ training state and label operator $O = |\Phi\rangle\langle\Phi|$, matching the canonical quantum compiling task. Thus, we can immediately give the overparameterization threshold for fidelity training of quantum generative models as $M_c \sim R_1$. Note as the full classical dataset is encoded into a single state, there is no explicit L dependence for overparameterization of fidelity training of quantum generative models.

Supplemental Materials I: Overparameterization of variational quantum eigensolver for eigenstates

The variational quantum eigensolver (VQE) finds the ground state of a Hamiltonian H [98]. This algorithm has been extended to find L low-energy eigenstates of H via the subspace-search variational quantum eigensolver (SSVQE) [83]. The idea of SSVQE is to select M -parameter ansatz $U(\boldsymbol{\theta})$, prepare L orthogonal basis states $\{|k\rangle\}_{k=1}^L$ and minimize the cost function

$$C(\boldsymbol{\theta}) = \sum_{k=1}^L w_k \langle k | U(\boldsymbol{\theta})^\dagger H U(\boldsymbol{\theta}) | k \rangle \quad (\text{S1})$$

where the weights $w_k \in (0, 1)$ are chosen as $w_k > w_{k+1}$. One can easily see that C is minimal when for all $k = 1, \dots, L$ we have $|\psi_k\rangle = U(\boldsymbol{\theta})|k\rangle$, where $|\psi_k\rangle$ is the eigenstate corresponding to the k -th lowest eigenvalue of H . Thus, by minimizing $C(\boldsymbol{\theta})$ we can find all L lowest eigenstates of H .

We now study overparameterization of the SSVQE as function of the number L of low-energy eigenstates to be found. For the case of finding only the ground state, i.e. $L = 1$, it is known that a generic VQE circuit ansatz becomes overparameterized for $M \sim 2^N$ parameters where training converges with high probability to the ground state [69].

We now use the DQFIM to determine overparameterization for $L > 1$ which to our knowledge has not been known. We assume that the Hamiltonian is non-degenerate so we can properly order eigenvalues. Then, we observe that training the SSVQE corresponds to a unitary learning problem where we must find the $U(\boldsymbol{\theta})$ that maps the $k = 1, \dots, L$ initial states $|k\rangle$ to their unique target states $|\psi_k\rangle = U(\boldsymbol{\theta})|k\rangle$. Thus, we argue that training the SSVQE requires the same critical number of parameters $M_c(L)$ for overparameterization for unitary learning problem. In particular, we have

$$M_c(L) = R_L(\rho_L, U(\boldsymbol{\theta}, M)) \quad (\text{S2})$$

where R_L is the maximal rank of the DQFIM and $\rho_L = L^{-1} \sum_{k=1}^L |k\rangle\langle k|$. For a generic ansatz unitary (for example composed of layers of parameterized single qubit rotations and CNOT gates), we get as derived in Sec. B

$$M_c^{\text{generic}}(L) = 2dL - L^2 - 1. \quad (\text{S3})$$

where $d = 2^N$ is the Hilbertspace dimension.

We now show numerical results on the SSVQE. We learn the L eigenstates with lowest energies of the Hamiltonian

$$H = \sum_j \sigma_j^x \sigma_{j+1}^x + g \sigma_j^x + h_j \sigma_j^z \quad (\text{S4})$$

with $g = 0.2$ and randomly chosen $h_j \in \{-1, 1\}$. We minimize the cost function Eq. (S1) until convergence (to either global or local minima). To evaluate the performance of the SSVQE, we compute the fidelity of the found states with the exact eigenstates via

$$F = \frac{1}{L} \sum_{k=1}^L |\langle \psi_k | U(\boldsymbol{\theta}^*) | k \rangle|^2 \quad (\text{S5})$$

where $\boldsymbol{\theta}^*$ is the parameter set found via training, $|\psi_k\rangle$ the eigenstate of H corresponding to the k th lowest eigenvalue. We show the converged function (minus the theoretical minimal possible value) as function of M and L in Fig. S11a. The dashed line is the maximal rank of the DQFIM R_L . We find that the cost function becomes very small once $M > R_L$, indicating the overparameterization transition. We show F in Fig. S11b, observing that the fidelity converges to 1 for $M > R_L$. Finally, we plot the number of training iterations needed to converge in Fig. S11c. We find that close to the overparameterization transition the training time increases, indicating that at the transition the optimization landscape is more complex [68].

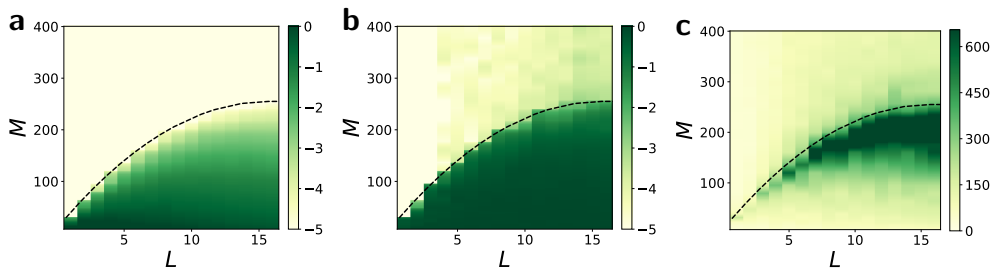


FIG. S11. Performance of SSVQE for finding lowest eigenstates of Hamiltonian Eq. (S4). **a**) Median of trained cost function $\log(C_{\text{train}} - C_{\text{min}})$ Eq. (S1) against circuit parameters M and number of eigenstates L . Dashed line is maximal rank of DQFIM R_L . **b**) Median of fidelity $\log(F)$. **c**) Number of training steps E until reaching $C_{\text{train}} < 10^{-4}$. We use generic ansatz U_{HE} of Fig.S1a with $N = 4$ qubits.

Supplemental Materials J: Overparameterization and generalization in classification tasks

We now consider a classification task with quantum machine learning. This is a supervised learning algorithm where one is given a classical training dataset $\{y_\ell, x_\ell\}$ with feature vector x_ℓ and binary label $y_\ell \in \{-1, +1\}$. The goal is to use the quantum computer to classify the data. This can be achieved by encoding the feature vector x_ℓ into a quantum state $|\psi(x_\ell)\rangle \equiv |\psi_\ell\rangle$. Then, one learns a parameterized unitary $U(\boldsymbol{\theta})$ such that the expectation value $\langle \psi_\ell | O_\ell | \psi_\ell \rangle$ in respect to an observable O_ℓ reproduces the label, i.e. we want to find $\boldsymbol{\theta}$ such that $\langle \psi_\ell | U^\dagger(\boldsymbol{\theta}) O_\ell U(\boldsymbol{\theta}) | \psi_\ell \rangle = y_\ell$ for all $\ell = 1, \dots, L$. A popular choice is $O_\ell = y_\ell \sigma^z$ with z Pauli operator σ^z . The corresponding quantum dataset is $S_L = \{|\psi_\ell\rangle, y_\ell \sigma^z\}_{\ell=1}^L$. The quantum classifier can be trained by minimizing the cost function [28]

$$C_{\text{train}}(\boldsymbol{\theta}) = 1 - \frac{1}{L} \sum_{\ell=1}^L \langle \psi_\ell | U^\dagger(\boldsymbol{\theta}) O_\ell U(\boldsymbol{\theta}) | \psi_\ell \rangle. \quad (\text{S1})$$

After training, the classifier is tested against unseen test data drawn from some distribution W to determine its generalization capability. For this, we can use the test error

$$C_{\text{test}}(\boldsymbol{\theta}) = 1 - \frac{1}{L} \sum_{\{|\psi\rangle\} \in W} \langle \psi | U^\dagger(\boldsymbol{\theta}) O_\psi U(\boldsymbol{\theta}) | \psi \rangle \quad (\text{S2})$$

with $O_\psi = y_\psi \sigma^z$ where y_ψ is the corresponding label to $|\psi\rangle$. When $C_{\text{test}} \approx 0$, we can optimally classify any test data, i.e. we are able to predict the correct label with only a single sampling of $\langle \psi | U^\dagger(\boldsymbol{\theta}) O_\psi U(\boldsymbol{\theta}) | \psi \rangle$.

What is a good choice for O to classify two classes of data? For the unitary learning problem $O = V|\psi\rangle\langle\psi|V^\dagger$ is a projector onto the target to be learned. Thus there is only one correct target state with $V|\psi\rangle = U(\boldsymbol{\theta})|\psi\rangle$ which is not useful for classification tasks. Commonly, for binary classification tasks one chooses O to be a Pauli operator, e.g. $O = \sigma_1^z$ [28]. This operator has two eigenvalues $+1, -1$ which can be used to distinguish the two classes. Now, one trains $U(\boldsymbol{\theta})$ such that it transforms data with $y = 1$ label to the $+1$ eigenspace of O , while data with $y = -1$ is transformed into the -1 eigenspace. Now, the solution space is highly degenerate as there are 2^{N-1} degenerate eigenvalues for each label. This makes the classification problem easier to learn in contrast to the unitary learning problem (which has only one correct solution), and classification problems require less parameters to overparameterize. Thus, the critical number of parameters $M_c(L)$ from the DQFIM presents an upper bound on overparameterization for classification tasks.

In the following, we study overparameterization numerically for classification. As we will see, the critical number of parameters M_c^{classify} is reduced compared to learning unitaries. In particular, we observe numerically that for σ_1^z we require $M_c^{\text{classify}} = R_L \gamma$ to overparameterize, where $\gamma \leq 1$. We observe that γ depends on the chosen circuit ansatz. In particular, for a generic ansatz circuit and σ^z we find $\gamma = \frac{1}{2}$, while for a particle-number conserving U_{XY} circuit we find $\gamma = \frac{1}{3}$.

We study the classification task in Fig. S12 for a generic ansatz circuit U_{HE} . In Fig. S12a, we show the classification training error C_{train} against circuit parameters M and training states L . We find that the training error becomes small when $M \geq R_L/2$ which is plotted as red line. This is half of the usual maximal rank of the DQFIM R_L which is also shown as black dashed line. While R_L describes overparameterization for unitary learning problems, for classification tasks with Pauli operators we find that overparameterization requires only half the number of circuit parameters. This is due to the degeneracy of the Pauli operator $O = \sigma_1^z$.

In Fig. S12b, we show the test error. We find generalization for $L \geq 16$, which is the same as for the unitary learning task. Finally, in Fig. S12c we show the number of training iterations needed to train. We find a peak in iterations for $M = R_L/2$.

Next, in Fig. S13 we study classification using the particle-number conserving U_{XY} ansatz of Fig. S1b. For this ansatz overparameterization scales polynomially with qubit number. In Fig. S13a we show the training cost against M, L . We find that training cost becomes small for $M \geq R_L/3$, which indicates a factor $\gamma = 1/3$ reduction compared to unitary learning. For the test error Fig. S13b we find generalization for $L \geq 2$, which is the same as for unitary learning.

Note that here we evaluated the test error by looking at C_{test} . One can also regard test error as the misclassification rate for the following decision rule: When $\langle \psi | U^\dagger(\boldsymbol{\theta}) O_\psi U(\boldsymbol{\theta}) | \psi \rangle \geq \epsilon$ we classify $y = 1$, and for $\langle \psi | U^\dagger(\boldsymbol{\theta}) O_\psi U(\boldsymbol{\theta}) | \psi \rangle \leq -\epsilon$ we classify as $y = -1$, with some threshold ϵ . C_{test} as defined in Eq. (S2) corresponds to the rule $\epsilon = 1$. Smaller ϵ can yield smaller generalization errors, however at the cost of increasing the number of measurement shots on the quantum computer $N_{\text{sample}} \sim 1/\epsilon^2$ as one needs to evaluate the observable $\langle \psi | U^\dagger(\boldsymbol{\theta}) O_\psi U(\boldsymbol{\theta}) | \psi \rangle$ to higher precision. The DQFIM

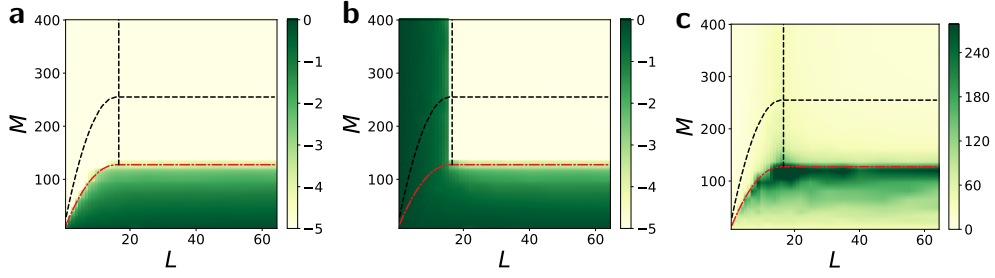


FIG. S12. Performance of classification task for generic circuit ansatz. **a)** Mean of trained cost function $\log(C_{\text{train}})$ against circuit parameters M and number of training states L . Black dashed line is maximal rank of DQFIM R_L , while red line is $R_L\gamma$ with empirical factor $\gamma = 1/2$. **b)** Median of test cost $\log(C_{\text{test}})$. **c)** Number of training steps E until reaching $C_{\text{train}} < 10^{-4}$. We use generic ansatz U_{HE} of Fig.S1a with $N = 4$ qubits, $O = \sigma_1^z$ as classification operator. States with label $y = 1$ are randomly drawn from a subspace with eigenvalue $+1$ of rotated operator $V\sigma_1^zV^\dagger$, while $y = -1$ from the -1 subspace.

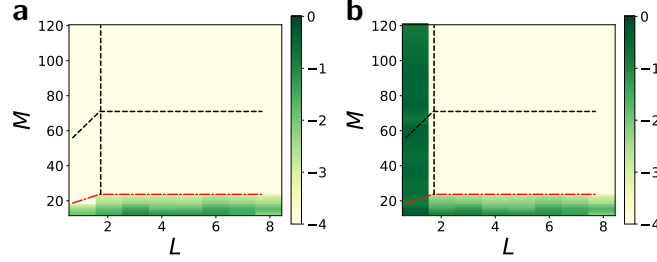


FIG. S13. Performance of classification task for particle-number conserving U_{XY} circuit. **a)** Mean of trained cost function $\log(C_{\text{train}})$ against circuit parameters M and number of training states L . Black dashed line is maximal rank of DQFIM R_L , while red line is $R_L\gamma$ with empirical factor $\gamma = 1/3$. **b)** Median of test cost $\log(C_{\text{test}})$. **c)** Number of training steps E until reaching $C_{\text{train}} < 10^{-4}$. We use U_{XY} ansatz of Fig.S1b with $N = 6$ qubits and $O = \sigma_1^z$ as classification operator. States with label $y = 1$ are randomly drawn from a subspace with eigenvalue $+1$ of rotated operator $V\sigma_1^zV^\dagger$, while $y = -1$ from the -1 subspace.

gives us the generalization threshold $L_c \sim 2R_\infty/R_1$ for the case $\epsilon = 1$. For smaller ϵ , $L_c(\epsilon) \leq L_{\text{extc}}(\epsilon = 1)$ is expected to decrease. Thus, generalization bound via the DQFIM can be seen as an upper bound on the number of datapoints needed to generalize.

Supplemental Materials K: Generalization and empirical generalization error

We define generalization via the error of the cost function C_{test} averages over the full data ensemble W . In our studies, we choose the problem such that $C_{\text{test}} = 0$ can be achieved for at least one parameter θ_g .

In general, the minimal achievable C_{test} for given ansatz and data distribution may not be known. Thus, often the empirical generalization error $\zeta = C_{\text{test}} - C_{\text{train}}$ of the trained model is used as a proxy to evaluate generalization [39]. In Fig. S14, we compare C_{train} , C_{test} and empirical generalization error $C_{\text{test}} - C_{\text{train}}$. We show the hardware-efficient ansatz with $N = 4$ overparameterizes for $M \geq M_c = 4^N - 1 = 255$ and $L_c = 2^N = 16$. When the model is underparameterized $M \leq M_c$, the training error in Fig. S14a and test error in Fig. S14b can be quite large. In contrast, the empirical generalization error in Fig. S14c shows favorable scaling with L . However, note that the actual test error decreases in absolute value only slightly with L . Overparameterization $M \geq M_c$ drastically reduces the training error to zero, and for $L \geq L_c$ allows us to find $C_{\text{test}} \approx 0$.

In Fig. S15 we study generalization and empirical generalization error for U_{XY} ansatz and symmetric data $W_{p=1}$. In Fig. S15a,b we see that C_{train} and C_{test} decreases with M , and reaches near-zero for $M \geq M_c$. In Fig. S15c we plot the empirical generalization error $\zeta = C_{\text{test}} - C_{\text{train}}$ against M . We find that ζ first increases, then decreases with M . We also note that ζ increases with N .

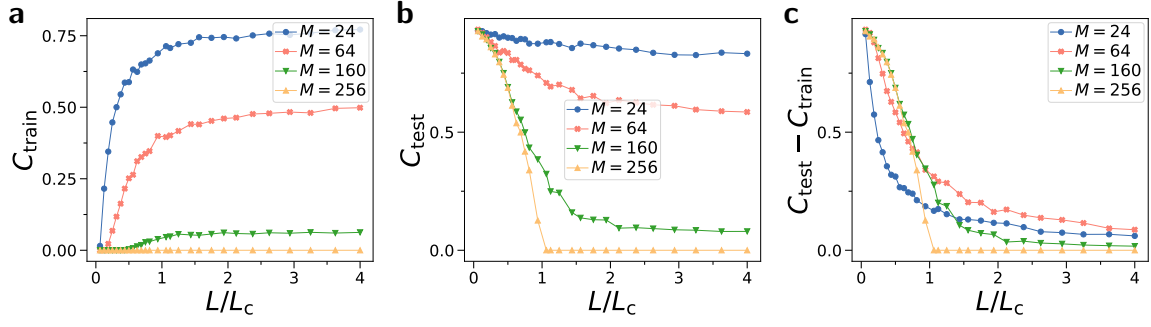


FIG. S14. Training error, test error and empirical generalization error for hardware-efficient ansatz with Haar random training states for $N = 4$ qubits. We assume that there is an optimal solution, i.e. there is at least one parameter with $C_{\text{test}}(\theta_g) = 0$. **a)** C_{train} against L for different M . **b)** C_{test} against L for different M . **c)** Empirical generalization error $C_{\text{test}} - C_{\text{train}}$ against L for different M .

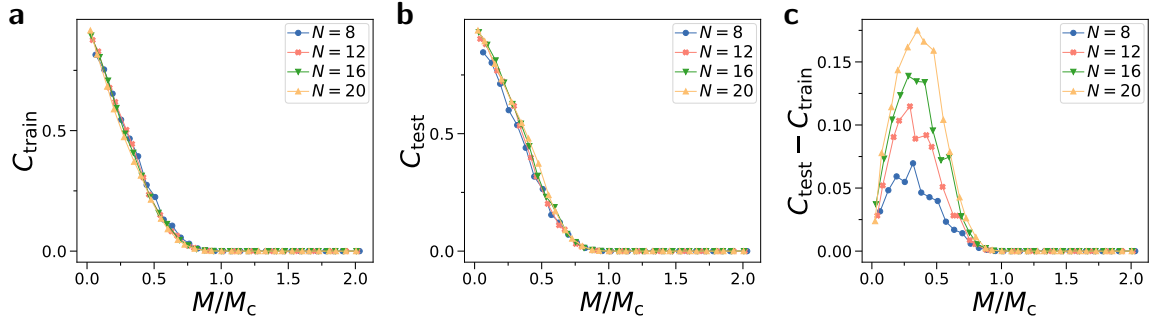


FIG. S15. Learning with U_{XY} and $|\psi_\ell\rangle \in W_{p=1}$ with fixed overcomplete data $L = 40 \gg L_c$ for $N = 16$. **a)** C_{train} against M for different N , where $M_c = N^2 - 1 = 255$. **b)** C_{test} against M for different N . **c)** Empirical generalization error $C_{\text{test}} - C_{\text{train}}$ against M .